SANDIA REPORT

SAND2009-5957
Unlimited Release
Printed September, 2009

Quantitative Resilience Analysis Through Control Design

Eric D. Vugrin, R. Chris Camphouse, and Daniel Sunderland

Prepared by
Sandia National Laboratories
Albuquerque, New Mexico 87185 and Livermore, California 94550

Sandia is a multiprogram laboratory operated by Sandia Corporation,
a Lockheed Martin Company, for the United States Department of Energy's
National Nuclear Security Administration under Contract DE-AC04-94-AL85000.

Approved for public release; further dissemination unlimited.

Sandia National Laboratories

Issued by Sandia National Laboratories, operated for the United States Department of Energy by Sandia Corporation.

NOTICE: This report was prepared as an account of work sponsored by an agency of the United States Government. Neither the United States Government, nor any agency thereof, nor any of their employees, nor any of their contractors, subcontractors, or their employees, make any warranty, express or implied, or assume any legal liability or responsibility for the accuracy, completeness, or usefulness of any information, apparatus, product, or process disclosed, or represent that its use would not infringe privately owned rights. Reference herein to any specific commercial product, process, or service by trade name, trademark, manufacturer, or otherwise, does not necessarily constitute or imply its endorsement, recommendation, or favoring by the United States Government, any agency thereof, or any of their contractors or subcontractors. The views and opinions expressed herein do not necessarily state or reflect those of the United States Government, any agency thereof, or any of their contractors.

Printed in the United States of America. This report has been reproduced directly from the best available copy.

Available to DOE and DOE contractors from
U.S. Department of Energy
Office of Scientific and Technical Information
P.O. Box 62
Oak Ridge, TN 37831

Telephone: (865) 576-8401
Facsimile: (865) 576-5728
E-Mail: reports@adonis.osti.gov
Online ordering: http://www.osti.gov/bridge

Available to the public from
U.S. Department of Commerce
National Technical Information Service
5285 Port Royal Rd
Springfield, VA 22161

Telephone: (800) 553-6847
Facsimile: (703) 605-6900
E-Mail: orders@ntis.fedworld.gov
Online ordering: http://www.ntis.gov/help/ordermethods.asp?loc=7-4-0#online

SAND2009-5957
Unlimited Release
Printed September, 2009

Quantitative Resilience Analysis Through Control Design

Eric D. Vugrin
Infrastructure and Economic Systems Analysis Department
Sandia National Laboratories
P.O. Box 5800
Albuquerque, NM 87185-1138
edvugri@sandia.gov

R. Chris Camphouse
Performance Assessment and Decision Analysis Department
Sandia National Laboratories
4100 National Parks Highway
Carlsbad, NM 88220
rccamph@sandia.gov

Daniel Sunderland
Systems Research, Analysis, and Applications Department
Sandia National Laboratories
P.O. Box 5800
Albuquerque, NM 87185-1138
dsunder@sandia.gov

Abstract

Critical infrastructure resilience has become a national priority for the U. S. Department of Homeland Security. System resilience has been studied for several decades in many different disciplines, but no standards or unifying methods exist for critical infrastructure resilience analysis. Few quantitative resilience methods exist, and those existing approaches tend to be rather simplistic and, hence, not capable of sufficiently assessing all aspects of critical infrastructure resilience. This report documents the results of a late-start Laboratory Directed Research and Development (LDRD) project that investigated the development of quantitative resilience through application of control design methods. Specifically, we conducted a survey of infrastructure models to assess what types of control design might be applicable for critical infrastructure resilience assessment. As a result of this survey, we developed a decision process that directs the resilience analyst to the control method that is most likely applicable to the system under consideration. Furthermore, we developed optimal control strategies for two sets of representative infrastructure systems to demonstrate how control methods could be used to assess the resilience of the systems to catastrophic disruptions. We present recommendations for future work to continue the development of quantitative resilience analysis methods.

Acknowledgments

We would like to thank Tom Corbet, Steve Conrad, and Angie Kelic for sharing their models and insights with the authors. We would also like to thank Drake Warren, Mark Ehlen, Adam Rose, and Tony Barrett for their discussions on resilience and for providing the economists' perspective. We also appreciate Bart van Bloemen Waanders perspectives on resilience and optimization. Finally, we would like to thank Munaf Aamir for taking the time to explain systems dynamics modeling techniques and conventions. His discussions were very helpful in the development of the supply-consumption model.

This work was supported by Laboratory Directed Research and Development funding from Sandia National Laboratories.

Contents

1 Introduction **13**

1.1 Resilience as a Homeland Security Mandate 13

1.2 A Quantitative Framework for Assessing Infrastructure and Economic Resilience 14

2 Model Issues and Control Selection for Resilience Analysis **17**

2.1 A Decision Process for Control Method Selection 17

2.2 Methodology Descriptions 18

2.2.1 PID Control 18

2.2.2 System Identification 20

2.2.3 Linear Optimal Feedback Control 20

2.2.4 Linearization 22

2.2.5 Nonlinear Control 22

2.2.6 Decentralized Control 22

2.2.7 Hybrid Control 23

2.3 Reduced Order Modeling: Proper Orthogonal Decomposition 23

3 Resilience Analysis of Representative Infrastructure Systems **27**

3.1 Supply-Consumption Systems 27

3.1.1 The Optimal Resilience Problem 29

3.1.2 Methodology 30

3.1.3 Resilience Analysis 30

3.1.4 Comparing the Resilience of a Multi-plant Supply-Consumption System Across Different Disruptions 32

3.1.5 Summary of Supply-Consumption System Analyses 34
3.2 Distributed Chemical Supply Chain 35
3.2.1 Numerical Discretization 37
3.2.2 Nominal and Disrupted Dynamics 39
3.2.3 Tracking Control 40
3.2.4 Controlled Results 41
3.2.5 Low-Dimensional Supply Chain Model 44
3.2.6 Reduced Model Results 48
3.2.7 Controlled Reduced Model 51
3.2.8 High-Dimensional Tracking 53

4 Summary and Future Work **56**

References **57**

List of Figures

2.1 A Model-Dependent Decision Process for Selecting a Control Method for Resilience Analysis 18

3.1 A Supply-Consumption System Represented with Systems Dynamic Conventions 28

3.2 Nominal Supply-Consumption Dynamics 31

3.3 Disrupted Supply-Consumption Dynamics: no emergency supply reserve 32

3.4 Disrupted Supply-Consumption Dynamics: with emergency supply reserve . . 33

3.5 Optimal Emergency Supply Rate 33

3.6 The Multi-Plant, Single Control Supply-Consumption System 34

3.7 Multiplant System Consumption Levels and Emergency Supply Rates for Two Disruption Scenarios 35

3.8 Distributed Chemical Supply Chain 36

3.9 Nominal Supply Chain Dynamics 39

3.10 Disrupted Supply Chain Dynamics 40

3.11 Departure of Species G from the Target Value After Disruption 40

3.12 Concentration Reference Profile 42

3.14 Departure of Species G from the Target Value After Disruption with Control 43

3.13 Disrupted Supply Chain Dynamics with Control 43

3.15 The Baseline and Actuator POD Bases 48

3.16 Reduced-Order Nominal Supply Chain Dynamics 49

3.17 Reduced-Order Disturbed Supply Chain Dynamics 50

3.18 Departure of Species G from the Target Value After Disruption for the Reduced Model 51

3.19 Concentration Reference Profile for the Reduced-Order Control Problem 52

3.20 Reduced-Order Disturbed Supply Chain Dynamics with Control 52

3.21 Departure of Species G from the Target Value After Disruption for the Reduced Model with Control 53

3.22 Controlled Full-Order Supply Chain Dynamics with Reduced-Order Control Implementation 54

3.23 Departure of Species G from the Target Value After Disruption for the Full-Order Model with Reduced-Order Control 55

List of Tables

3.1 System Parameters for Resilience Analysis 30

Chapter 1

Introduction

1.1 Resilience as a Homeland Security Mandate

U. S. Federal Government critical infrastructure protection (CIP) policies date back at least to the early 1980s, and, historically, these policies have focused on physical protection and asset hardening (for example, see [1], [2], [3], [4]). In 2005, U. S. Department of Homeland Security (DHS) Secretary Chertoff charged the Homeland Security Advisory Council to form the Critical Infrastructure Task Force (CITF) and to provide recommendations on national policy and objectives. The CITFs primary recommendation was that DHS focus on critical infrastructure resilience (CIR), a concept concerned with ensuring the optimal delivery of critical infrastructure service in an all hazards environment while simultaneously reducing the consequences of their exploitation, destruction, or disruption, as its top-level strategic objective.

The federal government has started a coordinated set of government resilience initiatives to begin the process of understanding what features create resilience in critical infrastructure/key resource (CIKR) systems. Agencies were called upon to start measuring the resilience of their infrastructure systems. The DHS National Infrastructure Protection Plan (NIPP), in particular, contains explicit language calling for increasing the resilience of the nation's critical infrastructure. Many of the NIPP sector-specific plans (SSPs) also have broad, if not specific, language that promotes critical infrastructure resilience as a primary objective.

The process of institutionalizing CIR analysis in federal policy faces many challenges. In particular, no uniform standards exist for conducting CIR analyses. Existing resilience assessment methodologies are generally not sufficient for CIR analysis. Current methods generally have one of the following shortcomings:

- The resilience assessment methods are domain- or model-specific, and, therefore, they are not applicable to all or any of DHS's 18 CIKR systems.
- The resilience methods focus on quantifying the impacts of a disruption to system output levels but do not consider the costs of system recovery. Vugrin et al. [5] assert that since recovery is a foundational component of resilience, suitable resilience assessment methods should explicitly consider recovery costs.

The development and adoption of a standardized approach that addresses these shortcomings for conducting CIR analysis is a critical step towards DHS's goal of better understanding resilient CIKR systems.

1.2 A Quantitative Framework for Assessing Infrastructure and Economic Resilience

In an effort to develop a uniform framework for CIR analysis, Vugrin et al. [6] have proposed the following definition of system resilience for use in CIR analysis:

Given the occurrence of a particular, disruptive event (or set of events), the resilience of a system to that event (or events) is that system's ability to efficiently reduce both the magnitude and duration of the deviation from targeted system performance levels.

According to this definition, *systemic impact* is measured as the difference between targeted system output levels and actual system output levels following a disturbance. The magnitude and duration of this disturbance are factors to be considered when quantifying systemic impact. The ability of the system to efficiently and rapidly return to targeted performance levels refers to the cost of system recovery, or what Vugrin et al. [5] term the *total recovery effort*.

Vugrin et al. [6] have further proposed the following approach for quantitatively assessing system resilience. Consider a dynamic system modeled as follows:

$$y(t) = f\left(x(u(t), d(t), t)\right), \tag{1.2.1}$$

where

- x is a state vector with dependence on the recovery effort u and the disturbance d.
- u is a time-dependent vector representing the means by which the system recovers, i.e., the recovery effort.
- d represents a time-dependent, piece-wise continuous, disturbance forcing term.
- y is the vector of system outputs under disturbance d, and is obtained by calculation of the function f.

Let y_{ref} be an exogenous reference signal that represents the time-dependent, targeted system performance level. If $t_0 > 0$ is the first time at which d is non-zero, i.e., the disturbance initiates, and t_1 is the first time at which system output levels return to targeted system performance levels following a disturbance, i.e., $y_{ref}(t_1) = y(t_1)$, then Vugrin et al. [6] define TRE, the total recovery effort, as

$$TRE = \int_{t_0}^{t_1} u^T R u \;\; dt, \tag{1.2.2}$$

The matrix R is an appropriately sized, positive definite weighting matrix. In general, the type of disturbance will dictate the recovery strategy. Thus, TRE is a function of d and u. Vugrin et al. [6] define SI, the systemic impact, as

$$SI = \int_{t_0}^{t_1} \left[y_{ref} - y\right]^T Q \left[y_{ref} - y\right] dt, \tag{1.2.3}$$

where Q is another appropriately sized, positive semi-definite weighting matrix.

The recovery dependent resilience costs, RDR, of x to d under u is defined as

$$RDR\left(x\left(t_0\right), u, d\right) = \frac{SI + TRE}{\int_{t_0}^{t_1} \left\{\left[y_{ref}\right]^T Q y_{ref}\right\} dt}. \tag{1.2.4}$$

The denominator in 1.2.4 is a normalizing term that permits comparison of RDR values for systems of varying magnitudes. When it exists, optimal resilience costs, OR, of system x to disturbance d is defined as

$$OR\left(x\left(t_0\right), d\right) = \min_u \frac{SI + TRE}{\int_{t_0}^{t_1} \left\{\left[y_{ref}\right]^T Q y_{ref}\right\} dt}. \tag{1.2.5}$$

The results of the recovery dependent and optimal resilience cost calculations are most informative when used in the following manner [5]:

- **The resilience costs for two different systems to the same disruption are compared**: The system with the lower resilience costs is the more resilient system to that disruption.
- **The resilience costs for one system to different disruption are compared**: The system is more resilient to the disruption that results in lower resilience costs.
- **The resilience costs for one system, to one disruption, and different recovery strategies are compared**: The recovery strategy that results in lower resilience costs will better enhance the system's resilience.

The approach proposed by Vugrin et al. [6] lends itself nicely to mathematical formulations utilized for the development of optimal feedback control laws. When applied to a system, feedback controllers utilize measured system outputs to regulate system behaviors to target conditions while simultaneously providing a measure of the cost in doing so. Incorporating feedback control in the quantitative description of resilience could enable automatic system recovery from disruption while providing a prediction of recovery cost.

As part of a late-start Laboratory Directed Research and Development (LDRD) project, we investigated the development of quantitative CIR analysis through the application of control, and optimal control, methods. Specifically, we sought to

- Investigate feasibility of quantitative CIR analysis through application of control methods.
- Identify appropriate control methods.
- Apply these control methods to evaluate resilience of representative infrastructure systems to catastrophic disruptions.

This report documents the outcome of that investigation.

The balance of this report is as follows. Chapter 2 contains the results of a survey of infrastructure models and control techniques that was conducted to evaluate the suitability of control methods for quantitative resilience analysis. As a result of this survey, a decision process was developed that directs CIR analysts to the control method that is most appropriate for their particular systems under consideration. The decision process is presented in Chapter 2, along with brief descriptions of the control techniques included as options in the decision process. Chapter 3 includes two examples of resilience analysis through application of optimal control methods to representative infrastructure systems. In the first application, we evaluate the resilience of a set of supply-consumption systems. We use these examples to quantitatively verify qualitative observations about resilience enhancement strategies. In the second application we consider a chemical supply chain prototype model. This system is modeled by a set of coupled partial differential equations. The number of states required to simulate this system is large and computationally intensive, a common challenge for modeling infrastructure systems. The purpose of this investigation is to demonstrate that reduced order modeling techniques, such as proper orthogonal decomposition (POD), can be used on high order systems and then combined with optimal control strategies to perform resilience analyses. The final chapter, Chapter 4, discusses follow-on work and analyses that should be considered in the further development of quantitative resilience methods that utilize control design techniques.

Chapter 2

Model Issues and Control Selection for Resilience Analysis

2.1 A Decision Process for Control Method Selection

This project began with the identification of prevalent issues associated with analyzing, modeling, and simulating infrastructure systems. Infrastructure models and modeling approaches used and developed by the National Infrastructure Simulation and Analyses Center (NISAC) were reviewed and assessed. Some of the issues associated with modeling infrastructure systems include:

- **Lack of a formal model**: In some instances resilience analysts do not have a formal model. They may have only a historical set of input/output data, or the details of a model may be proprietary and, therefore, unavailable, to the analyst. In the second instance, the model is essentially a "black box."
- **Nonlinearities**: Many infrastructure systems are inherently nonlinear. Linearization may simplify some of these models, but others may be highly nonlinear, and, thus, not suitable candidates for linearization.
- **Decentralized structure or "agent-based"**: Many infrastructure systems are best represented as networks of independent agents. The rules that dictate the behavior of these agents may be simple, but mathematical theory for analysis of these types of systems is not as developed as the theory developed for physics-based systems modeled with ordinary or partial differential equations.
- **High dimensionality**: Detailed infrastructure models can have thousands, even tens of thousands, of variables. These high dimensional systems can be computationally intensive, and, therefore, difficult to analyze through simulation. Large model dimension also leads to computational difficulties when utilizing optimal control design methods.

Given the spectrum of issues associated with modeling infrastructures, it is clear that no single control method is best for all types of infrastructure models. Hence, we developed a decision process that a resilience analyst can follow to evaluate the best control methodology

to apply to a specific infrastructure model (Figure 2.1). Completion of the process directs the analyst to the optimal control method that is most appropriate for performing resilience analysis on the model. The remainder of this chapter provides brief overviews of the control techniques that are a part of the decision process.

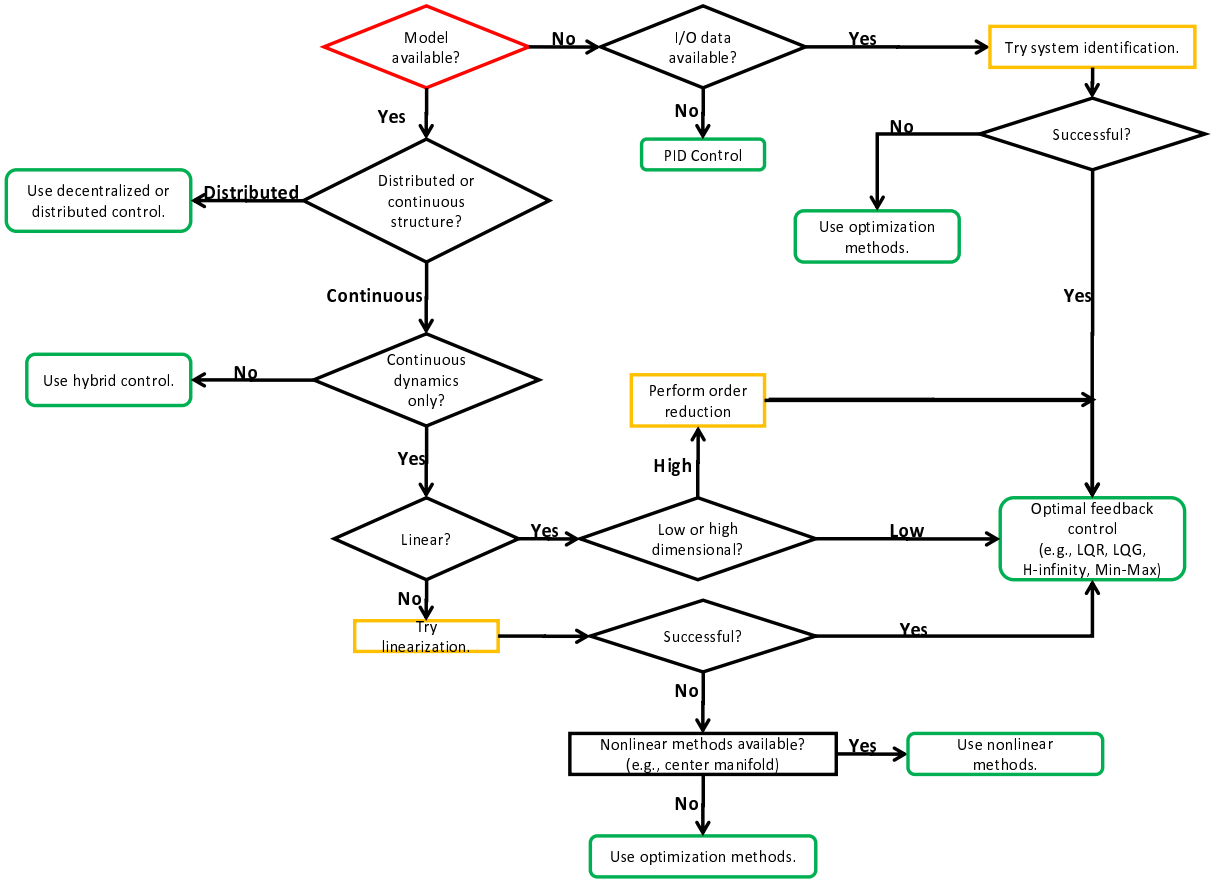

Figure 2.1. A Model-Dependent Decision Process for Selecting a Control Method for Resilience Analysis

2.2 Methodology Descriptions

2.2.1 PID Control

When possible, it is desirable to utilize a dynamical system model to develop controllers for a particular system of interest. However, it is often the case that a good model of the system is unavailable or is very difficult to develop. When a model is not available, controllers are often developed by use of a Proportional Integral Derivative (PID) control

design technique.

The use of PID controllers is widespread. The most common implementation of the PID controller is of the form

$$u(t) = K_P e(t) + K_I \int_0^t e(\tau)d\tau + K_D \frac{de(t)}{dt}. \tag{2.2.1}$$

In (2.2.1), u is the control signal and e is the tracking error between the system output and the desired output. As seen in (2.2.1), the typical PID controller is comprised of three terms. The first term is proportional to the tracking error. The second term is proportional to the integral of the tracking error. Finally, the third term is proportional to the time-derivative of the error. The three constants K_P, K_I, and K_D are gains placed on the three terms used to specify the controller. Their values are specified to place more or less emphasis on their corresponding terms in the control law.

Each of the three terms in the PID control law has a specific purpose. The first term adjusts the control input as a function of tracking error. Adjusting the proportional gain K_P results in a corresponding change in the tracking response. Care must be taken when specifying a value for K_P. Setting the proportional gain too high can result in small tracking errors having large impacts on the control input $u(t)$. Moreover, setting the gain too high may cause the closed-loop system to become unstable. Conversely, setting the proportional gain too low can result in small changes to the control input even if there is significant tracking error. In addition, with a gain that is too low, the control action may not be large enough to adequately respond to large system disturbances.

The proportional term by itself typically results in a steady-state tracking error. The addition of the integral term ensures that the system output tracks the reference condition in steady-state. When the integral term is included, positive steady-state tracking error results in a corresponding positive increase in the control input. Likewise, a negative steady-state tracking error yields a decrease in the control input.

The derivative term in the PID controller is included to improve closed-loop stability of the system. Multiplying the rate of change of the tracking error by the derivative gain K_D results in a controller that includes information about the predicted future tracking error. However, if the system output has signal noise associated with it, differentiating the tracking error can amplify the impacts of this noise. As a result, the derivative term is highly sensitive to noise in the tracking error measurement. This sensitivity can result in the closed-loop system becoming unstable if the noise and derivative gain are too large.

Many factors must be considered when specifying the PID gains K_P, K_I, and K_D. Moreover, the three terms in (2.2.1) are not always used to develop a feedback control for a particular system. The characteristics of the system, and potential noise associated with its measured output, dictate which terms in the PID control law are appropriate for the system at hand. A good reference for the design of PID feedback controllers is [7].

2.2.2 System Identification

System identification is another technique that can be used when a dynamical system model is not available. The main goal of system identification is to produce the *simplest* mathematical description that *adequately* predicts how the process responds to a given set of inputs [8]. An identified system may adequately predict process behaviors while utilizing a mathematical structure that is different from that of the actual process of interest [9].

In general, system identification requires a set of input and corresponding output data. Oftentimes, the modeler may have some idea about the structure of the model and parameters that need to be determined but not know the precise structure or values. System identification may be used to better understand the structure and assign parameter values. L. Ljung [10] provides a good introduction into system identification and related issues.

System identification is relevant to resilience analysis because it can be used to develop a mathematical description of a system when a model was not previously available. Frequently, system identification is used to develop a linear model. If this is possible, then linear optimal feedback control techniques can be applied to the resulting model.

2.2.3 Linear Optimal Feedback Control

When a dynamical model is available for a given system, it can often be expressed in a form suitable for linear control law design. Many systematic control formulations lend themselves to state-space system models of the form

$$\dot{X}(t) = AX(t) + Bu(t), t > 0, \tag{2.2.2}$$

$$X(0) = X_0(\mathbf{x}). \tag{2.2.3}$$

In (2.2.2), $X(t)$ is called the state vector with components $x_1(t)$, $x_2(t)$,...,$x_n(t)$ being state variables. Notation $\dot{X}$ denotes the differentiation of the state vector with respect to time. The control input to the system is denoted by $u(t)$. The coefficient matrices A and B are time invariant.

It is often required that state variables track a particular reference signal. A fixed reference signal $z(\mathbf{x})$ is specified, and it is desired that solutions of (2.2.2)-(2.2.3) track $z(\mathbf{x})$ as time evolves. As the tracking signal is time-invariant, the dynamics of the system and the reference signal are given by

$$\begin{bmatrix} \dot{X} \\ z \end{bmatrix} = \begin{bmatrix} A & 0 \\ 0 & 0 \end{bmatrix} \begin{bmatrix} X \\ z \end{bmatrix} + \begin{bmatrix} B \\ 0 \end{bmatrix} u \tag{2.2.4}$$

$$= \bar{A}\bar{X} + \bar{B}u, \tag{2.2.5}$$

where we have defined the augmented state $\bar{X}$ as $\bar{X} = [X \;\; z]^T$. The initial data of the augmented system is given by

$$\bar{X}_0 = \begin{bmatrix} X_0(\mathbf{x}) \\ z(\mathbf{x}) \end{bmatrix}. \tag{2.2.6}$$

It should be noted that (2.2.2)-(2.2.3) correspond to a linear system. A variety of optimal control techniques have been developed for linear systems. A particular example is that of the linear quadratic regulator (LQR) control formulation, which we now describe in detail.

The tracking formulation of the LQR control problem can be applied to the augmented state equation. For control scenarios where it is desired that state variables track a particular reference signal in steady-state, a cost function of the form

$$J(X_0, u) = \int_0^\infty \left\{(X - z)^T Q(X - z) + u^T R u\right\} dt \tag{2.2.7}$$

is used to develop the LQR feedback control. In (2.2.7), Q is a diagonal, symmetric, positive semi-definite matrix consisting of state weights. R is a diagonal, symmetric, positive definite matrix of control weights. The optimal control problem we consider is to minimize (2.2.7) over all controls $u \in L^2(0, \infty)$ subject to the constraints (2.2.4)-(2.2.6).

For a controllable system, the tracking LQR problem has a unique solution [8] of the form

$$\begin{aligned} u_{opt} &= -K\bar{X} && (2.2.8)\\ &= -[K_1 \;\; K_2]\bar{X} && (2.2.9)\\ &= -\left[R^{-1}B^T\Pi_{11} \;\; R^{-1}B^T\Pi_{12}\right]\bar{X}, && (2.2.10) \end{aligned}$$

where Π_{11} is the unique symmetric, non-negative solution of the algebraic Riccati equation

$$A^T\Pi_{11} + \Pi_{11}A - \Pi_{11}BR^{-1}B^T\Pi_{11} + Q = 0. \tag{2.2.11}$$

The matrix Π_{12} in (2.2.10) satisfies the equation

$$\left[A^T - \Pi_{11}BR^{-1}B^T\right]\Pi_{12} = Q. \tag{2.2.12}$$

There are many commercial software packages available that can solve the Riccati equation given by (2.2.11). With the Riccati matrix Π_{11} in hand, Π_{12} is found by simply solving matrix equation (2.2.12).

Once the gain matrix K is obtained, the feedback control law is placed into the augmented state-space equation. The resulting closed-loop system is of the form

$$\begin{aligned} \dot{\bar{X}} &= (\bar{A} - \bar{B}K)\bar{X}, && (2.2.13)\\ \bar{X}(0) &= \bar{X}_0. && (2.2.14) \end{aligned}$$

LQR is only one of several optimal control methods suitable for linear systems. Other techniques include linear quadratic Gaussian (LQG) optimal control, a method utilized when measurements are affected by "white, Gaussian noise" or if full state measurement is not possible. There are also robust control techniques, such as H-infinity control, that are used when it is necessary to stabilize a system in the presence of external disturbances. Zhou and Doyle [11] provides an excellent discussion of robust and optimal control methods for linear systems.

2.2.4 Linearization

It is often that case that a nonlinear system can be linearized about an equilibrium point with control subsequently designed from the linearized system. In this approach, the linearized model is a good representation of the nonlinear system inside some neighborhood about the equilibrium point. As a result, incorporating a feedback control law developed from the linearized system into the nonlinear plant can often give sufficient control performance inside the region of validity of the linearized model. The application of this approach to a nonlinear dynamical system can be found in [12].

2.2.5 Nonlinear Control

For some nonlinear systems, the stability of equilibria can not be determined by use of the linearized plant. As a result, the effectiveness of a control developed from the linearized plant is uncertain when placed in the original nonlinear model. For cases such as this, it is necessary to develop controls directly from the nonlinear model. Depending on the system under consideration, a combination of nonlinear control design tools may be required to provide effective control. Possible methods include sliding mode control, Lyopunov formulations, and applications of the celebrated Center Manifold Theorem. The use of these nonlinear control design techniques is outside the scope of this effort. Discussions of them can be found in [13].

2.2.6 Decentralized Control

Agent-based modeling is a commonly applied modeling technique applied to infrastructure systems. Agent-based models consist of a set of "agents" that interact with each other. Their interactions are generally determined by a set of simple rules. The agents generally behave in a manner that optimizes their own performance, rather than acting for the "greater good." Decentralized systems are often well suited for agent-based modeling approaches.

These types of systems and models often require *decentralized controllers*. In the decentralized control problem, agents generally have their own performance indices that they are attempting to maximize. Local controllers are developed based on the local dynamics, regulating the local behavior of agents [14]. A coordinator has a global performance index that is determined by the agents' local performance indices. Through the use of a decentralized control strategy, the coordinator attempts to optimize the global performance index. Sandell et al. [14] provides a good survey of decentralized control methods.

2.2.7 Hybrid Control

Many infrastructure models may exhibit radically different dynamics in different regions of the problem domain. For example, a dynamical model for an airplane may differ significantly during take-off and landing when compared to "cruise control" behavior at high altitudes. These types of models, termed hybrid models, can simultaneously display different types of dynamic behavior in different parts of the system [15]. This behavior frequently results a pairing of continuous elements with discrete planning algorithms or event-based elements (e.g., on-off switches).

These types of models require a type of control termed *hybrid-control*. Similar to the way dynamics of the system vary amongst different regions in the domain, controllers for hybrid systems vary from region to region. The references [16], [17], and [18] provide detailed discussions of hybrid systems and controllers for these systems.

2.3 Reduced Order Modeling: Proper Orthogonal Decomposition

Reduced-order modeling is often used to reduce the dimension of dynamical systems in order to lessen the burden of computation. Proper orthogonal decomposition (POD) is a popular order reduction technique that extricates a small set of optimal basis functions from large sets of observed system data. A POD algorithm [19, 20] based on the snapshot method [21] can be used to construct a low order basis suitable for the development of a reduced order system model. We now describe this basis construction technique. A data ensemble of snapshots $\{S_i(\mathbf{x})\}_{i=1}^N$ is generated for the system of interest via numerical simulation or experiment, where N is the total number of snapshots. Each snapshot consists of instantaneous system data. With the snapshot ensemble in hand, the $N \times N$ correlation matrix L defined by

$$L_{i,j} = \langle S_i, S_j \rangle \tag{2.3.1}$$

is constructed. In this work, we utilize the standard $L^2(\Omega)$ inner product

$$\langle S_i, S_j \rangle = \int_\Omega S_i S_j^* \mathbf{dx}, \tag{2.3.2}$$

where S_j^* denotes the complex conjugate of S_j, in the construction of L.

The eigenvalues $\{\lambda_i\}_{i=1}^N$ of L are calculated and sorted in descending order. The ratio

$$100 \left(\frac{\sum_{i=1}^M \lambda_i}{\sum_{i=1}^N \lambda_i} \right) \tag{2.3.3}$$

is used to determine the number of POD basis functions to construct. The quantity in (2.3.3) provides a measure of the ensemble variability that is captured by a POD basis consisting of

M modes. By requiring a percentage of the variability contained in the snapshot ensemble be contained in the basis, the smallest value of M is calculated such that the quantity in (2.3.3) is greater than or equal to that percentage.

The eigenvectors $\{v_i\}_{i=1}^{M}$ corresponding to the M eigenvalues of largest magnitude are calculated. Each eigenvector is normalized so that

$$\|v_i\|^2 = \frac{1}{\lambda_i}. \tag{2.3.4}$$

The orthonormal POD basis set $\{\phi_i(\mathbf{x})\}_{i=1}^{M}$ is constructed according to

$$\phi_i(\mathbf{x}) = \sum_{j=1}^{N} v_{i,j} S_j(\mathbf{x}), \tag{2.3.5}$$

where $v_{i,j}$ is the jth component of v_i. With the basis in hand, system states $X(t, \mathbf{x})$ are approximated as a linear combination of POD modes, i.e.,

$$X(t, \mathbf{x}) \approx \sum_{i=1}^{M} \alpha_i(t) \phi_i(\mathbf{x}). \tag{2.3.6}$$

Split-POD

Using an argument based on (2.3.3) is a convenient way to determine the number of POD modes to retain for a given system. However, blindly applying (2.3.3) to determine the necessary number of modes is problematic in many settings, particularly those with control action restricted to the system spatial domain boundary. In boundary control applications, it is desired that control input energy be as small as possible while still satisfying the control objective. Simply applying (2.3.3) to an ensemble consisting of baseline and boundary actuated data presents the risk of important system information due to control input being discarded. System behaviors induced by boundary actuation often have much lower energy content than those associated with the baseline dynamics. For these reasons, the POD algorithm described above was extended in [22] so that baseline and control input energy are considered separately. This method is referred to as split-POD. The basis resulting from this method consists of modes significant to the baseline dynamics as well as those significant from an actuation standpoint.

The basic idea of split-POD is to decompose each snapshot in the ensemble into a component in the span of a baseline POD basis and an orthogonal component. This is done by employing useful properties of orthogonal projections on Hilbert spaces [23]. By considering the case of baseline and actuated data separately, the orthogonal component is constructed such that it contains new information due to the control input.

An ensemble of solution snapshots is generated for the case of zero control input. From this baseline snapshot ensemble, a set of POD modes is constructed that contains a high

percentage of the baseline variability. For notational convenience, denote this baseline basis by $\{\xi_j\}_{j=1}^{\bar{M}_B}$ where $\bar{M}_B$ is the number of modes. By employing the ratio in (2.3.3), $\bar{M}_B$ is chosen so that the baseline basis contains most of the variability contained in the baseline snapshot ensemble.

With a large set of baseline modes in hand, an ensemble of solution snapshots is generated for the case of nonzero control input. Denote the actuated ensemble by $\{T_i\}_{i=1}^{N_A}$ where N_A is the number of actuated snapshots.

The component that is in the span of the baseline basis is determined for each snapshot in the actuated ensemble. In particular, define b_{ij} according to

$$b_{ij} = \langle T_i, \xi_j \rangle, 1 \leq i \leq N_A, 1 \leq j \leq \bar{M}_B. \tag{2.3.7}$$

Then, b_{ij} is the projection of the ith actuated snapshot T_i onto the jth baseline POD mode ξ_j. In other words, the product $b_{ij}\xi_j$ is the component of T_i that is in the direction of ξ_j. The linear combination $\sum_{j=1}^{\bar{M}_B} b_{ij}\xi_j$ is the component of T_i in the span of the baseline basis.

Define $\bar{T}_i$ according to

$$\bar{T}_i = T_i - \sum_{j=1}^{\bar{M}_B} b_{ij}\xi_j. \tag{2.3.8}$$

Then, $\bar{T}_i$ is the component of T_i not contained in the span of the high order baseline basis. As T_i is a solution snapshot for the case of nonzero control input, $\bar{T}_i$ consists of new information due to the control input. A second set of POD modes is constructed from the data ensemble $\{\bar{T}_i\}_{i=1}^{N_A}$. This set of "actuator modes" is denoted by $\{\eta_i\}_{i=1}^{M_A}$, where M_A is the number of modes. The ratio in (2.3.3) is used to determine M_A such that the basis of actuator modes contains an arbitrary amount of the additional variability resulting from the control input. The high order baseline basis was employed to extricate new information resulting from the control. Having done that, the baseline basis is truncated to contain a more reasonable number of modes for model development. Denote M_B as the number of baseline modes retained after truncation with corresponding basis set $\{\xi_j\}_{j=1}^{M_B}$

To simplify reduced order modeling, it is advantageous to use a basis consisting of orthonormal modes. It is shown in [22] that the sets of baseline and actuator modes can be combined into an overall basis set

$$\{\phi_i\}_{i=1}^{M_B+M_A} = \{\xi_1, \xi_2, ..., \xi_{M_B}, \eta_1, \eta_2, ..., \eta_{M_A}\}, \tag{2.3.9}$$

where all modes in the basis are orthonormal. The system states $X(t, \mathbf{x})$ are still approximated as a linear combination of modes as in (2.3.6). Moreover, separate consideration of baseline and actuated system data allows us to write this linear combination as

$$X(t, \mathbf{x}) \approx \sum_{j=1}^{M_B} \theta_j(t)\xi_j(\mathbf{x}) + \sum_{i=1}^{M_A} \beta_i(t)\eta_i(\mathbf{x}), \tag{2.3.10}$$

where $\{\theta_j\}_{j=1}^{M_B}$ and $\{\beta_i\}_{i=1}^{M_A}$ are temporal coefficients for the baseline and actuator basis, respectively. This allows system states to be represented as the summation of a baseline component and an additional component induced by the control input.

The split-POD technique can be used to construct an optimal low-dimensional basis from experimental as well as simulated data. This technique is combined with PID control to develop feedback controllers from collected wind tunnel data in [24] for a hemispherical turret application. Its impact on LQR control effectiveness is demonstrated in [22] for a nonlinear dynamical system in simulation.

Chapter 3

Resilience Analysis of Representative Infrastructure Systems

In this chapter we present example demonstrations of resilience analysis through control design for a set of representative infrastructure systems. The first set of systems are relatively simple supply-consumption systems, and we examine the resilience of these systems to supply disruptions before and after resilience enhancements are made to the systems. We additionally consider a distributed chemical supply chain analogue. The system is complex,and the model for this system involves thousands of state variables. We investigated the resilience of this system to demonstrate that resilience analysis could be applied to large, computationally intensive models. We applied reduced-order modeling techniques in order to perform the analysis.

3.1 Supply-Consumption Systems

The first system that we consider, a modification of Sterman's stock management structure [25](see Figure 17-4) is shown in Figure 3.1. This model represents a relatively simple supply-consumption system, and we use systems dynamics modeling techniques to represent the dynamics of the system. In this system, the rate of consumption, C, of a commodity is the sum of the loss rate, LR, of a stock, S, and the rate at which an emergency supply, ESR, can supply that commodity to the consumer. The acquisition rate, AR, for the stock is the sum of the expected consumption rate, EC, and a stock adjustment strategy, AS, that attempts to have stock levels track a desired stock profile, S^*. The stock loss rate is proportional to the inventory of the stock. For this system, the emergency supply rate represents the control term. The emergency supply is intended to be activated when the consumption cannot meet the external demand signal.

We use the following set of equations to model the supply-consumption system:

$$\frac{d}{dt}S(t) = AR(t) - LR(t), \tag{3.1.1}$$

$$\frac{d}{dt}C(t) = LR(t) + ESR(t). \tag{3.1.2}$$

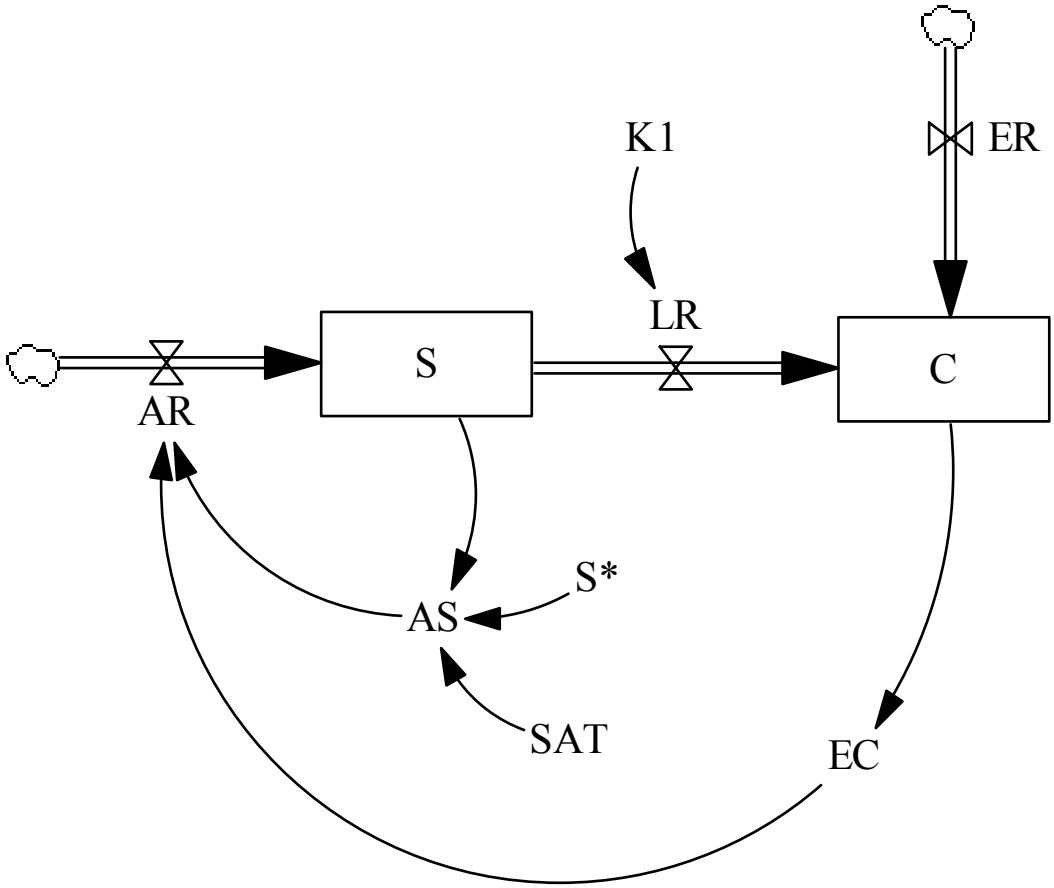

Figure 3.1. A Supply-Consumption System Represented with Systems Dynamic Conventions

The variables AR and LR are defined as follows:

$$LR = k1S, \tag{3.1.3}$$

where $k1$ is a proportionality constant, and

$$AR = SA + EC. \tag{3.1.4}$$

The stock manager's adjustment strategy, SA, is defined as

$$SA = \frac{S^* - S}{SAT}. \tag{3.1.5}$$

The constant SAT represents the stock adjustment time.

Estimated consumption is the average consumption over a fixed time period. It is calculated according to

$$EC = \frac{C(t) - C(t - td)}{td}. \tag{3.1.6}$$

The term t_d is the period over which consumption is averaged.

These variables can be combined into a two-dimensional, differential-delay equation that describes the entire system:

$$\frac{d}{dt}\begin{bmatrix} S(t) \\ C(t) \end{bmatrix} = A_0 \begin{bmatrix} S(t) \\ C(t) \end{bmatrix} + A_1 \begin{bmatrix} S(t-td) \\ C(t-td) \end{bmatrix} + \begin{bmatrix} 1 \\ 0 \end{bmatrix} N(t) + \begin{bmatrix} 0 \\ 1 \end{bmatrix} ESR(t), \tag{3.1.7}$$

where

$$A_0 = \begin{bmatrix} -1/SAT - k_1 & 1/td \\ k1 & 0 \end{bmatrix}, \tag{3.1.8}$$

$$A_1 = \begin{bmatrix} 0 & -1/td \\ 0 & 0 \end{bmatrix}, \tag{3.1.9}$$

and $N(t)$ represents a potential disturbance to the system. The measured output, y, for the system is calculated

$$y(t) = \begin{bmatrix} 0 & 1 \end{bmatrix} \begin{bmatrix} S(t) \\ C(t) \end{bmatrix} = C(t). \tag{3.1.10}$$

3.1.1 The Optimal Resilience Problem

For the supply-consumption system, we consider the following set of resilience analysis questions:

- Given the dynamics of the supply-consumption system described in equations (3.1.1) - (3.1.10), what are the resilience costs of a system, as defined in equation (3.1.11) with no emergency supply to a particular disruption?

  $$J(S(0), C(0), ESR) = \frac{\int_0^\infty [C(t) - D(t)]^2 \, dt}{\int_0^\infty [D(t)]^2 \, dt} + \frac{\int_0^\infty R\,[ESR(t)]^2 \, dt}{\int_0^\infty [D(t)]^2 \, dt}, \tag{3.1.11}$$

  In (3.1.11), $D(t)$ represents an exogenous demand signal and R is a scalar constant that balances the cost of the systemic impact, $C(t) - D(t)$ with the recovery effort $ESR(t)$.

- For that same system, what are the resilience costs when an emergency supply is available?

- What is the optimal emergency supply strategy that minimizes the resilience costs and maximizes the system's resilience to the disruption?

As discussed in [5], we observe that the addition of the emergency supply should enhance the absorptive capacity of the system, thus increasing the system's resilience. We now perform a resilience analysis to quantitatively verify this hypothesis.

3.1.2 Methodology

To perform the resilience analysis, we utilized LQR optimal feedback control described in Section 2.2.3. This approach is well-suited to this particular system since the model is linear. The system is infinite dimensional due to the delay term, $C(t - td)$. Hence, in order to perform simulation, the system must be approximated and discretized. We used the averaging scheme described in [26], [27], and [28] to do so. This approximation methodology was selected as feedback control approximations developed with the averaging scheme have been shown to converge (in norm) to the optimal control for the infinite dimensional system [28] and [29]. Kappel [28] describes in detail how to develop the matrices required for the LQR methodology.

Empirical testing indicated that relatively low order ($N \approx 4$) approximations sufficiently represent the solution. As a result, reduced-order modeling methods were not necessary to decrease the order of the system.

3.1.3 Resilience Analysis

Table 3.1 lists the system parameter values that we used for the resilience analysis. Additionally, equations (3.1.12) and (3.1.13) define the history functions (i.e., how $S(t)$ and $C(t)$ are evaluated over $[-td, 0))$ and S^*.

Table 3.1. System Parameters for Resilience Analysis

Parameter	Value
SAT	8
td	1
$k1$	0.25

We evaluated the resilience of two supply-consumption systems. The first is the supply-consumption system when no emergency supply exists, i.e., $ESR = 0$. The second system is identical with the exception that it has an emergency supply. The addition of the emergency supply is expected to enhance the absorptive capacity of the system, and consequently, the system with the emergency supply should be more resilient than the system without.

$$S(t) = 1/2\left[1 + \sin(t)\right], \quad t \in [-1, 0), \tag{3.1.12}$$

$$S^*(t) = 1/2\left[1 + \sin(t)\right]. \tag{3.1.13}$$

Figure 3.2 shows the dynamics of the supply-consumption system for undisrupted conditions. The dynamics are identical with and without the emergency supply. Figure 3.3 displays the dynamics of the system without an emergency supply when we impose a dis-

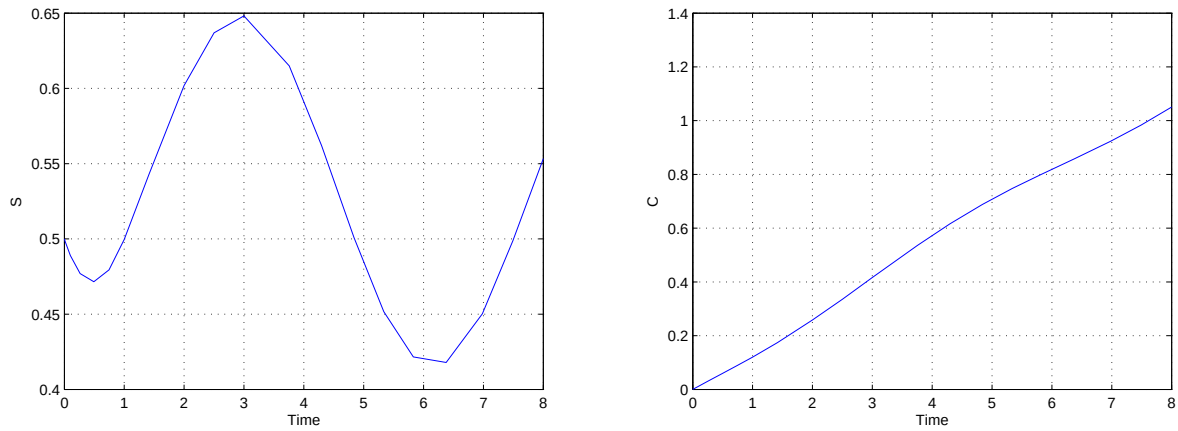

(a) Nominal Dynamics for the Stock S

(b) Nominal Dynamics for Consumption C

Figure 3.2. Nominal Supply-Consumption Dynamics

ruption $N(t)$ (defined in equation (3.1.14) to the acquisition rate.

$$N(t) = \begin{cases} -1, & 1 \leq t \leq 1.2, \\ 0, & \text{otherwise} \end{cases} \tag{3.1.14}$$

Stock levels drop sharply as soon as the disruption occurs. When the disruption ends, the gap between disrupted and undisrupted stock levels decreases, but stock levels never attain undisrupted levels. The decrease in stock leads to a decrease in the consumption rate, which affects the expected consumption rate. (Recall that the expected consumption rate is determined by averaging the consumption rate.) Disrupted consumption levels never reach nominal consumption levels, and the gap between the two increases over time. The consumption rate is directly proportional to the stock level, so decreased stock levels result in decreased consumption rates, causing the growing gap between disrupted consumption levels and nominal consumption levels.

Figure 3.4 shows the stock and consumption levels for the system with the emergency supply in place. The rate at which the emergency supply is utilized is determined through an LQR control design that attempts to make the disrupted consumption levels track demand levels (D in equation (3.1.11)) that are equal to the nominal consumption levels. In this figure, we see that the disrupted consumption levels decrease relative to the nominal consumptions immediately following the disruption. However, the control term (shown in Figure 3.5), prevents that decrease from reaching the disrupted consumption levels that were seen when no emergency supply was available. Furthermore, the gap between the consumption levels for the nominal case and the disrupted case with emergency supply does not increase following the disruption.

The resilience costs, as calculated with equation (3.1.11), for the supply-consumption

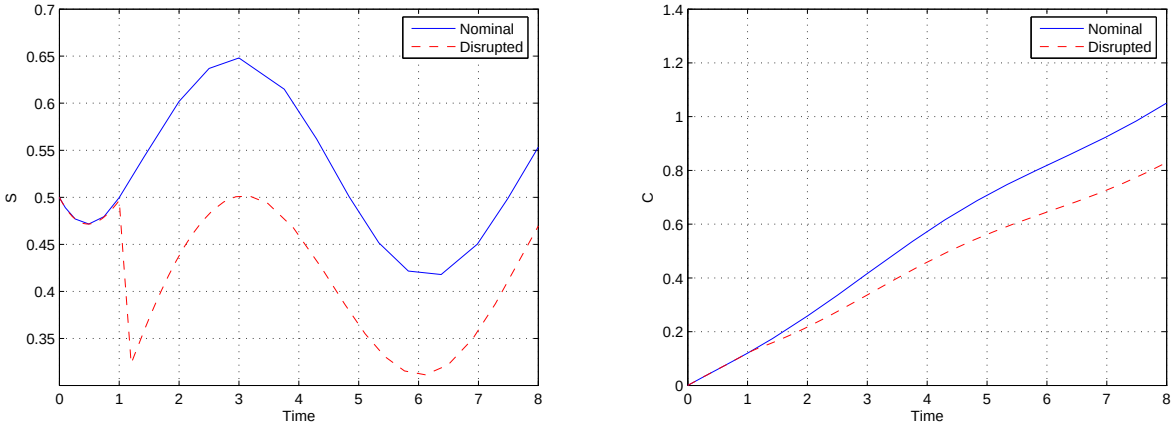

(a) Nominal Dynamics for the Stock S

(b) Nominal Dynamics for Consumption C

Figure 3.3. Disrupted Supply-Consumption Dynamics: no emergency supply reserve

system without an emergency supply are 7E-3 (unitless). The resilience costs for the supply-consumption system with the emergency supply were decreased to 7E-5 (unitless). Hence, in this example, we are able to quantitatively demonstrate that the addition of the emergency supply decreases resilience costs and, therefore, increases the resilience of the system to this disruption.

3.1.4 Comparing the Resilience of a Multi-plant Supply-Consumption System Across Different Disruptions

Figure 3.6 shows a variation of the previously considered supply-consumption model. This system is a "multi-stock, single control" system in which four stocks feed the consumption term, and one emergency supply reserve can supplement the supply from the four stocks when a disruption affects one or more of them. (The dynamics for the individual stocks are identical to the dynamics of the stock in the previous example, so system parameters for the individual stocks are identical to the parameters in Table 3.1.)

Under nominal conditions in the "multi-stock, single control" system, all plants run at near capacity; one plant provides 75 percent of the nominal consumption rate, two plants provide 10 percent each of the nominal consumption rate, and one plant provides 5 percent of the consumption rate.

We considered the resilience of this system to two types of disruptions. In the first disruption scenario, the acquisition rate to the largest plant is disrupted. In the second disruption scenario, the acquisition rate to smallest plant is identically disrupted. One

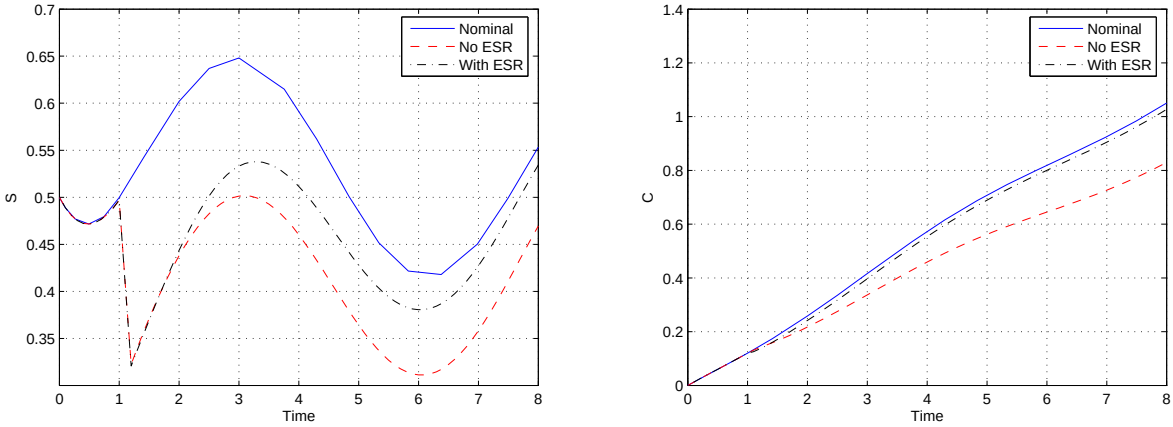

(a) Stock S Dynamics with ESR

(b) Consumption C Dynamics with ESR

Figure 3.4. Disrupted Supply-Consumption Dynamics: with emergency supply reserve

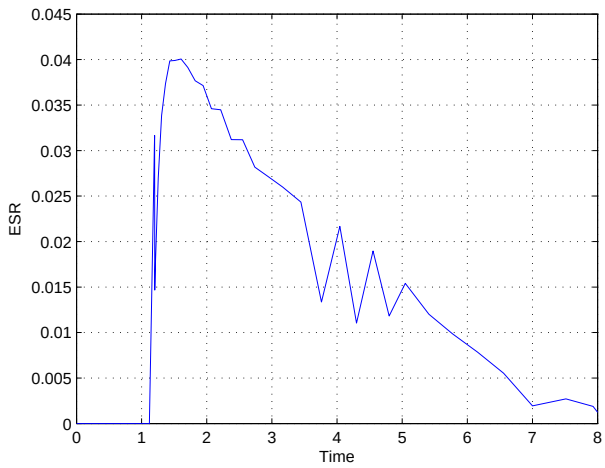

Figure 3.5. Optimal Emergency Supply Rate

would expect that the system will be more resilient to the second type of disruption than the first type.

The simulations confirm that hypothesis. Consumption levels for the two scenarios are indistinguishable, and track the nominal consumption fairly well (Figure 3.7(a)). However, the amount of emergency supply required to maintain these consumption levels are much

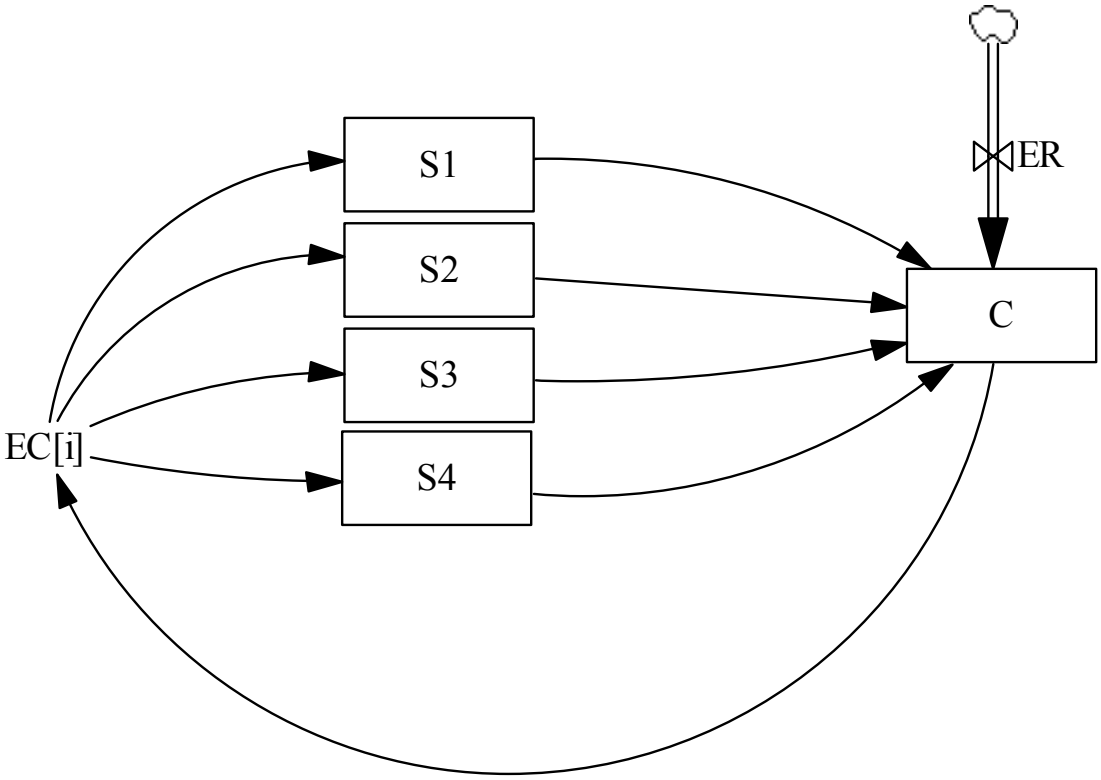

Figure 3.6. The Multi-Plant, Single Control Supply-Consumption System

higher for Scenario 1 when the larger plant is disrupted (Figure 3.7(b)). Though the two systems have similar system impacts, the total recovery costs resulting from the use of the emergency supplies are larger for the first scenario. Hence, the system is more resilient to the second type of disruption that affects the smallest plant.

3.1.5 Summary of Supply-Consumption System Analyses

In the supply-consumption system, we quantitatively evaluated resilience in two different ways. In the first configuration, we compared the resilience of two different systems: one without an emergency supply of a commodity and one with an emergency supply. This emergency supply was expected to enhance the absorptive capacity of the system and lead to greater resilience. We subjected both systems to identical disruptions, and through application of optimal control laws, we were not only able to quantitatively support this hypothesis, but we also identified the optimal strategy that best utilized the emergency reserve.

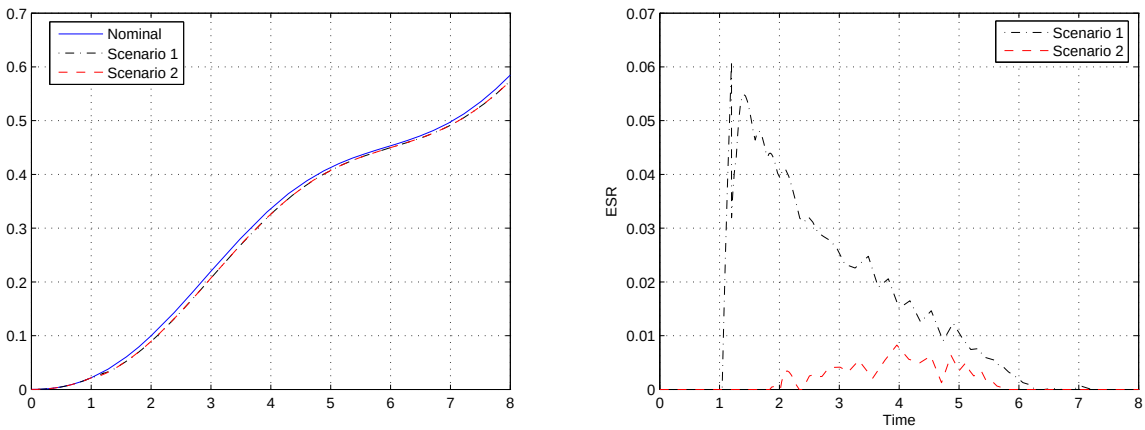

(a) Scenario 1: disrupt the largest plant

(b) Scenario 2: disrupt the smallest plant

Figure 3.7. Multiplant System Consumption Levels and Emergency Supply Rates for Two Disruption Scenarios

In the second evaluation, we compared the resilience of a multi-plant, single emergency reserve system to two types of disruption scenarios. In the first scenario, the acquisition rate of the largest plant was negatively affected. In the second scenario, the smallest plant's acquisition rate was identically impacted. Though the system impacts were nearly identical for the two scenarios, the total recovery cost, or cumulative control, for the first scenario was much higher. Hence, the resilience costs for the first scenario are larger, and the system is more resilient to the second type of disruption.

3.2 Distributed Chemical Supply Chain

Many physical processes that are important from an infrastructure resilience standpoint have dynamics that vary spatially as well as temporally. These dynamics can often be modeled by partial differential equations with appropriate initial and boundary conditions. Advantages gained by incorporating feedback control methods in the quantitative resilience methodology are now illustrated in a chemical supply chain configuration described by a set of coupled partial differential equations. A schematic illustrating the supply chain is shown in Figure 3.8. The supply chain is comprised of five chemical species V, W, F, G, and H with their concentrations denoted by C_V, C_W, C_F, C_G, and C_H, respectively. The chemical concentrations vary with time and space, and their evolution is described by a set of five coupled partial differential equations over the spatial interval $[0, L]$. These equations are of

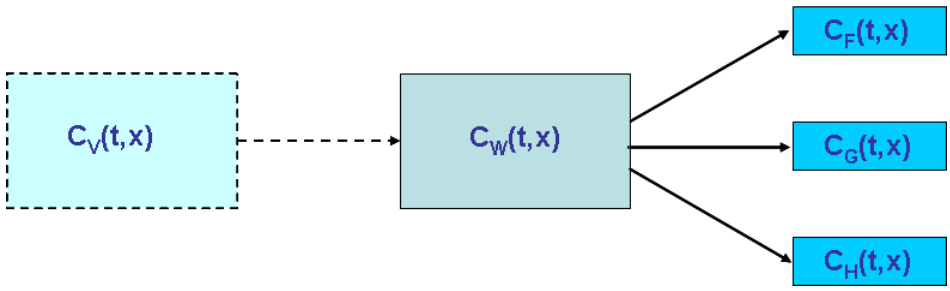

Figure 3.8. Distributed Chemical Supply Chain

the form

$$\frac{\partial}{\partial t}C_V(t,x) = \epsilon\frac{\partial^2}{\partial x^2}C_V(t,x) - \mu\frac{\partial}{\partial x}C_V(t,x) - k_V C_V(t,x), \tag{3.2.1}$$

$$\frac{\partial}{\partial t}C_W(t,x) = \epsilon\frac{\partial^2}{\partial x^2}C_W(t,x) - \mu\frac{\partial}{\partial x}C_W(t,x) + y_W k_V C_V(t,x) - k_W C_W(t,x), \tag{3.2.2}$$

$$\frac{\partial}{\partial t}C_F(t,x) = \epsilon\frac{\partial^2}{\partial x^2}C_F(t,x) - \mu\frac{\partial}{\partial x}C_F(t,x) + y_F k_W C_W(t,x) - k_F C_F(t,x), \tag{3.2.3}$$

$$\frac{\partial}{\partial t}C_G(t,x) = \epsilon\frac{\partial^2}{\partial x^2}C_G(t,x) - \mu\frac{\partial}{\partial x}C_G(t,x) + y_G k_W C_W(t,x) - k_G C_G(t,x), \tag{3.2.4}$$

$$\frac{\partial}{\partial t}C_H(t,x) = \epsilon\frac{\partial^2}{\partial x^2}C_H(t,x) - \mu\frac{\partial}{\partial x}C_H(t,x) + y_H k_W C_W(t,x) - k_H C_H(t,x), \tag{3.2.5}$$

for $t > 0$ and $x \in (0, L]$. In (3.2.1) - (3.2.5), the constants k_V, k_W, k_F, k_G, and k_H are first order reaction rates. Stoichiometric yield factors are denoted by y_W, y_F, y_G, and y_H. Species dispersion is prescribed by the constant ϵ. Finally, μ is a velocity parameter, which we take to be constant for the sake of simplicity in what follows.

In the supply chain configuration, the desired mode of operation is for species W to dissociate into the three daughter products F, G, and H. The target operating condition is for daughter concentration $C_G(t,x)$ to be at a specific value at $x = L$. Under normal operating conditions, this target value is attained by specifying a nominal value of $C_W(t,x)$ at $x = 0$. This nominal value results in a concentration profile of species W along the interval $[0, L]$ that yields the desired concentration of daughter product G at $x = L$. The resulting boundary condition at $x = 0$ for the concentration of species W is of the form

$$C_W(t,0) = f(t), \tag{3.2.6}$$

where $f(t)$ is the (possibly) time-varying nominal value of $C_W(t,x)$ at $x = 0$ that provides the desired concentration of species G at $x = L$.

Chemical species V has species W as a daughter product. As a result, species V is used as an emergency supplier of species W in the event that species W has a disruption in its availability. In other words, the concentration of species V at $x = 0$ is used as a control

input to the supply chain. The resulting boundary condition is of the form

$$C_V(t,0) = u(t), \tag{3.2.7}$$

where $u(t)$ is the time-varying closed-loop input to the system that automatically compensates for disruptions in the supply of $C_W(t,0)$. In the nominal operating condition, $u(t)$ remains held at a value of zero. Under disrupted operating conditions, $u(t)$ becomes nonzero to keep the concentration of species G at its target value at $x = L$ until the concentration $C_W(t,0)$ returns to its nominal value $f(t)$.

Homogeneous conditions are specified for the concentrations of species F, G, and H at $x = 0$. The resulting boundary conditions are of the form

$$C_F(t,0) = 0, \tag{3.2.8}$$
$$C_G(t,0) = 0, \tag{3.2.9}$$
$$C_H(t,0) = 0. \tag{3.2.10}$$

A Robin boundary condition is specified for the five species concentrations at $x = L$, resulting in

$$\begin{aligned} &rC_V(t,L) + \frac{\partial}{\partial x}C_V(t,L) = 0, && rC_W(t,L) + \frac{\partial}{\partial x}C_W(t,L) = 0, \\ &rC_F(t,L) + \frac{\partial}{\partial x}C_F(t,L) = 0, && rC_G(t,L) + \frac{\partial}{\partial x}C_G(t,L) = 0, \\ &rC_H(t,L) + \frac{\partial}{\partial x}C_H(t,L) = 0, \end{aligned} \tag{3.2.11}$$

for a constant $r \geq 0$.

Finally, the model is completed with initial species concentrations in $L^2([0,L])$.

3.2.1 Numerical Discretization

The infinite-dimensional system given by (3.2.1) - (3.2.11) is discretized utilizing a finite difference scheme. As we aim to utilize model-based control design methods to develop feedback controllers, the discretized system we desire is in the form of a state-space model. The interval $[0,L]$ is uniformly partitioned with spatial step-size h. The resulting grid nodes are denoted by $x_1, x_2, ..., x_N$. Second-order discretizations are used for both the first and second-order spatial derivatives in (3.2.1) - (3.2.5). In addition, a second-order discretization is used for the first-order spatial derivatives in the Robin conditions in (3.2.11). Utilizing these discretizations results in a system of ordinary differential equations approximating the

model given by (3.2.1) - (3.2.11). The discretized system is of the form

$$\begin{bmatrix} \dot{C_V} \\ C_W \\ C_F \\ C_G \\ C_H \end{bmatrix} = \begin{bmatrix} A_{C_V} & 0 & 0 & 0 & 0 \\ y_W k_V I & A_{C_W} & 0 & 0 & 0 \\ 0 & y_F k_W I & A_{C_F} & 0 & 0 \\ 0 & y_G k_W I & 0 & A_{C_G} & 0 \\ 0 & y_H k_W I & 0 & 0 & A_{C_H} \end{bmatrix} \begin{bmatrix} C_V \\ C_W \\ C_F \\ C_G \\ C_H \end{bmatrix} + \begin{bmatrix} B_{C_V} \\ 0 \\ 0 \\ 0 \\ 0 \end{bmatrix} u_V(t) + \begin{bmatrix} 0 \\ F_{C_W} \\ 0 \\ 0 \\ 0 \end{bmatrix} f(t), \tag{3.2.12}$$

which we simply write in the state-space representation

$$\dot{C} = AC + Bu + Ff \tag{3.2.13}$$

$$C(0) = C_0(x). \tag{3.2.14}$$

In (3.2.12), I denotes the $N \times N$ identity matrix. The matrices A_{C_V}, A_{C_W}, A_{C_F}, A_{C_G}, and A_{C_H} are tridiagonal matrices of dimension $N \times N$. The matrices B_{C_V} and F_{C_W} separate the influence of time-varying boundary conditions in the model and are of dimension $N \times 1$. In (2.2.2), the vector C has dimension $5N \times 1$. The matrix A is of dimension $5N \times 5N$. The control matrix B has dimension $5N \times 1$. Forcing vector F is also of dimension $5N \times 1$.

3.2.2 Nominal and Disrupted Dynamics

To illustrate the impacts of disruption on the ability of the default supply chain (without control) to maintain its target output, nominal and disrupted supply chain dynamics are now compared. In the results that follow, species dispersion ϵ is prescribed a value of 10. First order reaction rates k_V, k_W, k_F, k_G, and k_H are given values of 0.2, 0.1, 0.02, 0.02, and 0.02, respectively. Stoichiometric yield factors of $y_W = 0.5$, $y_F = 0.3$, $y_G = 0.2$, and $y_H = 0.1$ are specified. The velocity parameter μ is set to 0.4. The behavior of the supply chain without disruption, a nominal value of $f(t) = 1$, and a target value of $C_G(t, L) = 0.0372$ with $L = 40$, is shown in Figure 3.9. In Figure 3.9(b), the desired concentration of species G is denoted by

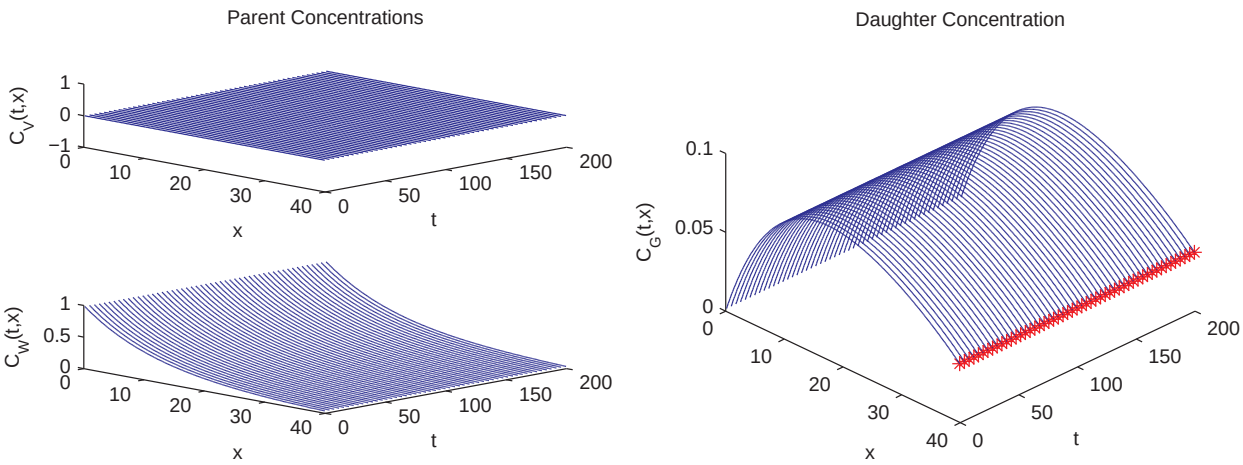

(a) Nominal Dynamics for Species V and W

(b) Nominal Dynamics for Species G

Figure 3.9. Nominal Supply Chain Dynamics

the asterisks at $x = 40$ in the plot of $C_G(t, x)$. As is evident, the target value is maintained well under the undisturbed nominal operating condition. In this condition, the emergency supply V is not required for the target performance level to be met, as seen in Figure 3.9(a).

The supply of concentration W at $x = 0$ is now severely disrupted. At $t = 5$, species W undergoes a catastrophic failure, with its available supply at $x = 0$ being completely eliminated. The supply of species W does not begin to recover until $t = 75$, when it is gradually brought back online to its nominal value. The behavior of the disturbed supply chain with no control is shown in Figure 3.10. As seen in Figure 3.10(b), the severe disruption in the supply of species W causes the concentration of daughter species G to severely depart from its target value at $x = 40$. The impact of the disruption on the supply chain is more clearly seen in Figure 3.11. In that figure, the dashed curve denotes the desired value of $C_G(t, 40)$. The solid curve denotes the value attained for $C_G(t, 40)$ for the disrupted supply chain. Obviously, the disruption causes $C_G(t, 40)$ to depart significantly from its target value.

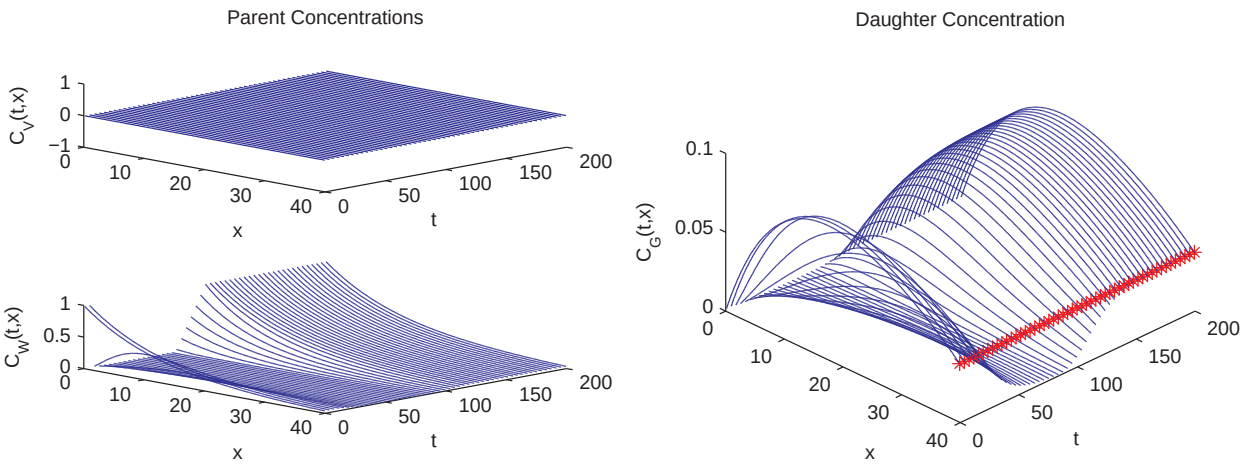

(a) Disturbed Dynamics for Species V and W

(b) Disturbed Dynamics for Species G

Figure 3.10. Disrupted Supply Chain Dynamics

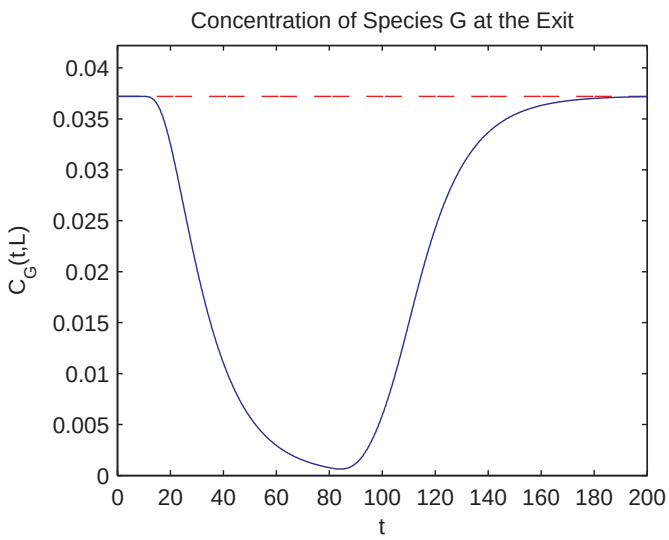

Figure 3.11. Departure of Species G from the Target Value After Disruption

3.2.3 Tracking Control

We now formulate a feedback control formulation with the aim of holding $C_G(t, L)$ at its target value, even during a disruption in the availability of species W. As discussed

previously, the concentration of species V at $x = 0$ is the control input to the system. As the control input enters the system via a boundary condition, the corresponding control formulation designates a boundary control problem. The need to hold $C_G(t, L)$ at a target value corresponds to tracking control. As seen in (3.2.1) - (3.2.5), the governing equations that describe the system are linear. For the chemical supply chain configuration discussed in this section, a tracking LQR control formulation is used to obtain the boundary feedback control $u(t)$. To this end, steady-state target reference concentrations are specified of the form

$$C_{ref} = \left[C_{V_{ref}} C_{W_{ref}} C_{F_{ref}} C_{G_{ref}} C_{H_{ref}}\right]^T. \tag{3.2.15}$$

As the reference concentrations do not vary with time, the dynamics of the species concentrations and the reference signals are given by

$$\begin{bmatrix} \dot{C} \\ C_{ref} \end{bmatrix} = \begin{bmatrix} A & 0 \\ 0 & 0 \end{bmatrix} \begin{bmatrix} C \\ C_{ref} \end{bmatrix} + \begin{bmatrix} B \\ 0 \end{bmatrix} u + \begin{bmatrix} F \\ 0 \end{bmatrix} f \tag{3.2.16}$$

$$= \bar{A}\bar{C} + \bar{B}u + \bar{F}f, \tag{3.2.17}$$

where we have defined the augmented state $\bar{C}$ as

$$\bar{C}(t) = \begin{bmatrix} C(t) \\ C_{ref} \end{bmatrix} \text{ with } \bar{C}(0) = \begin{bmatrix} C_0 \\ C_{ref} \end{bmatrix}. \tag{3.2.18}$$

The tracking LQR problem is solved, and the resulting optimal feedback control is placed into augmented state-space equation (3.2.17). The resulting closed-loop system is of the form

$$\dot{\bar{C}} = (\bar{A} - \bar{B}K)\bar{C} + \bar{F}f \tag{3.2.19}$$

$$\bar{C}(0) = \bar{C}_0. \tag{3.2.20}$$

The LQR controller can take values that are either positive or negative. There is nothing in the tracking LQR formulation that restricts the control input to non-negative values. The control input to the supply chain is the concentration of species V at $x = 0$. As such, a negative value for the controller does not make physical sense as it corresponds to a negative concentration. To account for this, negative values for the controller are replaced by a value of zero during implementation.

3.2.4 Controlled Results

We now demonstrate the increase in supply chain resilience due to the incorporation of feedback control. The steady-state concentration profile for species G obtained in the nominal operating condition is used for the reference profiles in (3.2.15). This reference profile is shown in Figure 3.12. As seen in Figure 3.12, the reference profile has the target value of 0.0372 at $x = 40$.

As the control objective is only concerned with the tracking of $C_G(t, x)$, states corresponding to the other four chemical concentrations are prescribed state-weights of zero in

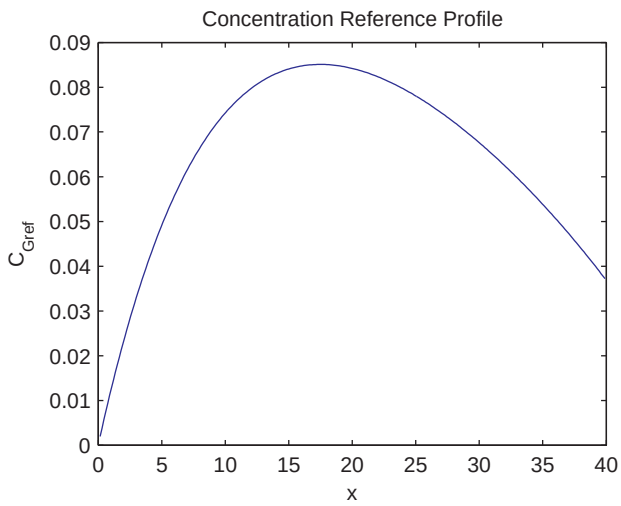

Figure 3.12. Concentration Reference Profile

LQR cost function (2.2.7). To isolate the concentration of species G near $x = 40$ in the control problem, values of $C_G(t, x)$ over the interval $[39.6, 40]$ are prescribed state-weights of 5.0×10^9. Values of $C_G(t, x)$ outside of this interval are given state-weights of zero. Unit weight is specified for the control input in the definition of R. The behavior of the disturbed chemical supply chain with incorporated feedback control is shown in Figure 3.13. As seen in Figure 3.13(a), species V turns on after failure to force the necessary profile in its daughter chemical, species W. This allows for the target value of $C_G(t, 40)$ to be maintained, even during the severe disruption to the nominal operating condition. The improvement in the supply chain resilience is easily seen by comparing the results of Figure 3.13(b) to the uncontrolled results seen in Figure 3.10(b). With incorporated feedback control, the target condition is held quite well during the disruption whereas the uncontrolled supply chain deviates severely.

The ability of the feedback control to maintain the target condition, even during a severe disruption, is more clearly seen in Figure 3.14. As is evident by comparing the results of Figure 3.14 and Figure 3.11, incorporating feedback control allows for much better performance during disruption, and increases the resilience of the chemical supply chain. As species W is gradually brought back to its nominal value after $t = 75$, species V gradually vanishes from the system and eventually returns to zero.

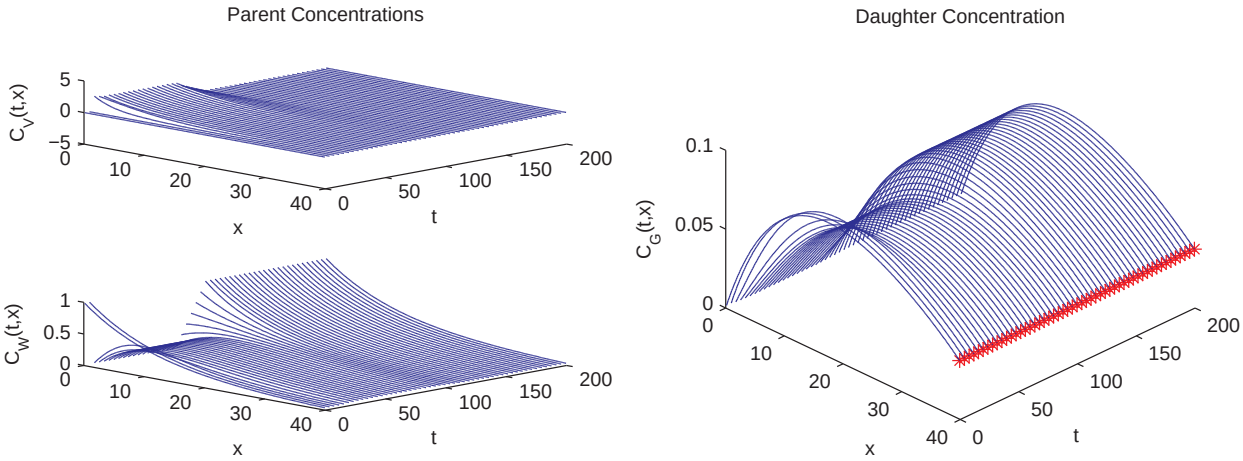

(a) Disturbed Dynamics for Species V and W with Control

(b) Disturbed Dynamics for Species G with Control

Figure 3.13. Disrupted Supply Chain Dynamics with Control

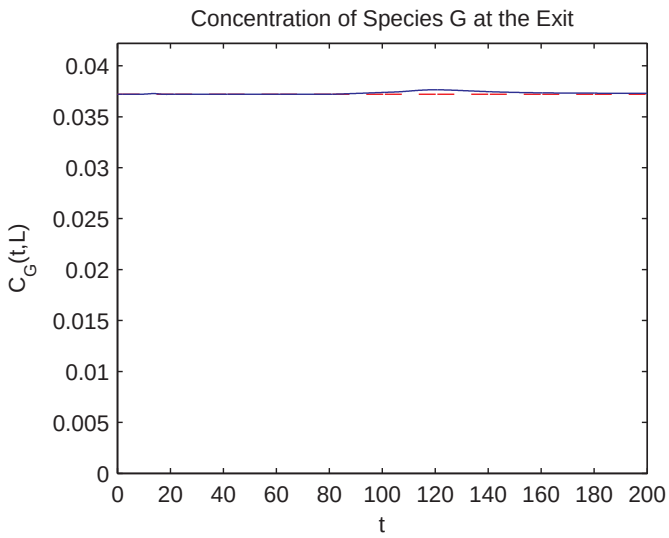

Figure 3.14. Departure of Species G from the Target Value After Disruption with Control

3.2.5 Low-Dimensional Supply Chain Model

Extending the feedback control techniques utilized in this section to highly discretized, multi-dimensional spatial domains or to supply chain configurations comprised of many chemical species introduces computational challenges. As the number of states described by the supply chain model becomes very large, numerically calculating the solution to the algebraic Riccati equation becomes problematic. Solving the Riccati equation requires finding a matrix solution that satisfies the nonlinear equation in (2.2.11). The Riccati solution matrix is symmetric. Thus, calculating it requires that $n(n+1)/2$ matrix unknowns be solved for, where n is the number of states in the system. As n becomes large, the calculation of the Riccati solution becomes intractable. Order reduction of the system model is required for cases such as these. Proper orthogonal decomposition has been successfully combined with weakly formed Galerkin projections to reduce dynamical system order and obtain low-dimensional state-space representations [30, 31, 32, 33]. These order reduction techniques also lend themselves to nonlinear control methods where low system order is critical [34, 35]. To demonstrate the utility of these ideas for chemical supply chain configurations, we now develop a reduced-order model for the supply chain described by (3.2.1) - (3.2.11). The split-POD technique is used to construct an overall basis consisting of optimal baseline and actuator modes. With the basis set in hand, the five chemical species concentrations are represented as linear combinations of these modes. The basis mode expansions are of the form

$$C_V(t,x) \approx \sum_{i=1}^{N_V} \alpha_i(t)\phi_i(x), \tag{3.2.21}$$

$$C_W(t,x) \approx \sum_{i=1}^{N_W} \beta_i(t)\phi_i(x), \tag{3.2.22}$$

$$C_F(t,x) \approx \sum_{i=1}^{N_F} \xi_i(t)\phi_i(x), \tag{3.2.23}$$

$$C_G(t,x) \approx \sum_{i=1}^{N_G} \eta_i(t)\phi_i(x), \tag{3.2.24}$$

$$C_H(t,x) \approx \sum_{i=1}^{N_H} \theta_i(t)\phi_i(x), \tag{3.2.25}$$

where N_V, N_W, N_F, N_G, and N_H are the number of modes used in the expansion of each species concentration. The scalars $\alpha_i(t)$, $\beta_i(t)$, $\xi_i(t)$, $\eta_i(t)$, and $\theta_i(t)$ are the temporal coefficients used in the POD expansions of concentrations $C_V(t,x)$, $C_W(t,x)$, $C_F(t,x)$, $C_G(t,x)$, and $C_H(t,x)$, respectively.

The reduced-order model for the distributed parameter system describing the chemical supply chain is now developed. The aim is to reduce the infinite-dimensional system given by (3.2.1) - (3.2.11) to a small set of ordinary differential equations. As the boundary conditions for $C_W(t,x)$ and $C_V(t,x)$ at $x = 0$ are time-varying, we need boundary conditions (3.2.6)

and (3.2.7) to be explicit in the reduced model. We make these conditions explicit during order reduction by forming the weak Galerkin projection of each governing equation onto the POD basis. We begin with species concentration $C_V(t,x)$.

Taking the $L^2([0,L])$ inner product of governing equation (3.2.1) with the i-th POD mode $\phi_i(x)$ results in a variational equation of the form

$$\int_0^L \dot{C}_V(t,x)\phi_i(x)dx = \epsilon \int_0^L C_V''(t,x)\phi_i(x)dx - \mu \int_0^L C_V'(t,x)\phi_i(x)dx - k_V \int_0^L C_V(t,x)\phi_i(x)dx. \tag{3.2.26}$$

Boundary conditions are made explicit by constructing the weak formulation of (3.2.26). Integrating by parts yields

$$\int_0^L C_V''(t,x)\phi_i(x)dx = C_V'(t,L)\phi_i(L) - C_V'(t,0)\phi_i(0) - \int_0^L C_V'(t,x)\phi_i'(x)dx \tag{3.2.27}$$

$$\approx -rC_V(t,L)\phi_i(L) - \left[\frac{C_V(t,h)-u(t)}{h}\right]\phi_i(0) - \int_0^L C_V'(t,x)\phi_i'(x)dx, \tag{3.2.28}$$

where the Robin condition in (3.2.11) has been used to replace $C_V'(t,L)$ by $-rC_V(t,L)$. In addition, $C_V'(t,0)$ has been replaced by a forward difference approximation with $h>0$. This allows us to make time-varying boundary condition (3.2.7) explicit. In the results that follow, h is prescribed to be the spatial step-size used in the finite difference discretization of the distributed parameter system.

In a similar fashion, integration by parts provides that

$$\int_0^L C_V'(t,x)\phi_i(x)dx = C_V(t,L)\phi_i(L) - u(t)\phi_i(0) - \int_0^L C_V(t,x)\phi_i'(x)dx, \tag{3.2.29}$$

where boundary condition (3.2.7) has been used to replace $C_V(t,0)$ by $u(t)$.

Substituting (3.2.28) and (3.2.29) into (3.2.26) results in the weak formulation

$$\int_0^L \dot{C}_V(t,x)\phi_i(x)dx = -\phi_i(L)C_V(t,L)(\epsilon r+\mu) - \frac{\epsilon}{h}C_V(t,h)\phi_i(0)$$
$$+ \int_0^L \left[\left(\mu C_V(t,x) - \epsilon C_V'(t,x)\right)\phi_i'(x) - k_V C_V(t,x)\phi_i(x)\right]dx + \left[\left(\mu + \frac{\epsilon}{h}\right)\phi_i(0)\right]u(t). \tag{3.2.30}$$

Approximating $C_V(t,x)$ as a linear combination of orthonormal POD modes as in (3.2.21)

results in a Galerkin system of the form

$$\dot{\alpha}_i(t) =$$
$$\sum_{j=1}^{N_V}\left[-\phi_i(L)\phi_j(L)(\epsilon r+\mu)-\frac{\epsilon}{h}\phi_j(h)\phi_i(0)+\int_0^L\left\{\left(\mu\phi_j(x)-\epsilon\phi_j^{'}(x)\right)\phi_i^{'}(x)-k_V\phi_j(x)\phi_i(x)\right\}dx\right]\alpha_j(t)$$
$$+\left[\left(\mu+\frac{\epsilon}{h}\right)\phi_i(0)\right]u(t), \qquad i=1,2,...,N_V. \tag{3.2.31}$$

The system of ordinary differential equations in (3.2.31) is written as a matrix equation of the form

$$\dot{\alpha} = A_\alpha\alpha + B_\alpha u(t), \tag{3.2.32}$$

where

$$A_\alpha(i,j) = -\phi_i(L)\phi_j(L)(\epsilon r+\mu)-\frac{\epsilon}{h}\phi_j(h)\phi_i(0)+\int_0^L\left\{\left(\mu\phi_j(x)-\epsilon\phi_j^{'}(x)\right)\phi_i^{'}(x)-k_V\phi_j(x)\phi_i(x)\right\}dx, \tag{3.2.33}$$

$$B_\alpha = \left(\mu+\frac{\epsilon}{h}\right)\begin{bmatrix}\phi_1(0)\\ \phi_2(0)\\ \cdot\\ \cdot\\ \cdot\\ \phi_{N_V}(0)\end{bmatrix}, \tag{3.2.34}$$

for $i,j = 1,2,...,N_V$.

The development of the weak Galerkin system for the remaining four chemical species is similar. However, as seen in governing equations (3.2.2) - (3.2.5), the remaining species are coupled. Concentration $C_W(t,x)$ is coupled to concentration $C_V(t,x)$ via the stoichiometric yield factor y_W. Similarly, concentrations $C_F(t,x)$, $C_G(t,x)$, and $C_H(t,x)$ are coupled to concentration $C_W(t,x)$ via the stoichiometric yield factors y_F, y_G, and y_H, respectively. This coupling results in a slightly more complicated Galerkin system for the four remaining concentrations.

Proceeding as before, it follows that the weak formulation for concentration $C_W(t,x)$ is of the form

$$\int_0^L \dot{C}_W(t,x)\phi_i(x)dx = -\phi_i(L)C_W(t,L)(\epsilon r+\mu)-\frac{\epsilon}{h}C_W(t,h)\phi_i(0)+\left[\left(\mu+\frac{\epsilon}{h}\right)\phi_i(0)\right]f(t)$$
$$+\int_0^L\left[\left(\mu C_W(t,x)-\epsilon C_W^{'}(t,x)\right)\phi_i^{'}(x)-k_W C_W(t,x)\phi_i(x)+y_W k_V C_V(t,x)\phi_i(x)\right]dx. \tag{3.2.35}$$

As seen by comparing (3.2.30) and (3.2.35), the coupling of concentration $C_W(t,x)$ to $C_V(t,x)$ results in an additional term in the integrand of the weak formulation.

Approximating $C_W(t,x)$ and $C_V(t,x)$ as linear combinations of POD modes as in (3.2.21) - (3.2.22) results in

$$\dot{\beta}_i(t) =$$

$$\sum_{j=1}^{N_W}\left[-\phi_i(L)\phi_j(L)(\epsilon r+\mu)-\frac{\epsilon}{h}\phi_j(h)\phi_i(0)+\int_0^L\left\{\left(\mu\phi_j(x)-\epsilon\phi_j^{'}(x)\right)\phi_i^{'}(x)-k_W\phi_j(x)\phi_i(x)\right\}dx\right]\beta_j(t)$$

$$+\left[\left(\mu+\frac{\epsilon}{h}\right)\phi_i(0)\right]f(t)+y_Wk_V\sum_{m=1}^{N_V}\left[\int_0^L\phi_m(x)\phi_i(x)dx\right]\alpha_m(t),\qquad i=1,2,...,N_W. \tag{3.2.36}$$

The system of ordinary differential equations in (3.2.36) is written as a matrix equation of the form

$$\dot{\beta}=A_\beta\beta+F_\beta f(t)+I_\beta\alpha. \tag{3.2.37}$$

In (3.2.37), matrix A_β has dimension $N_W\times N_W$, and is analogous to the matrix A_α in (3.2.33) with k_V replaced by k_W. Matrix F_β has dimension $N_W\times 1$, and is akin to matrix B_α in (3.2.34). Matrix I_β has dimension $N_W\times N_V$. Due to the orthonormality in $L^2([0,L])$ of modes used in the POD expansion, elements of I_β are of the form

$$I_\beta(i,j)=\begin{cases}y_Wk_V, & \text{when } i=j,\\ 0, & \text{otherwise}\end{cases} \tag{3.2.38}$$

for $i=1,2,...,N_W$ and $j=1,2,...,N_V$.

The systems for daughter concentrations $C_F(t,x)$, $C_G(t,x)$, and $C_H(t,x)$ are found in a similar fashion. As these concentrations are held at zero at $x=0$, their matrix equations are of the form

$$\dot{\xi}=A_\xi\xi+I_\xi\beta, \tag{3.2.39}$$

$$\dot{\eta}=A_\eta\eta+I_\eta\beta, \tag{3.2.40}$$

$$\dot{\theta}=A_\theta\theta+I_\theta\beta. \tag{3.2.41}$$

Matrix A_ξ, A_η, and A_θ have dimensions $N_F\times N_F$, $N_G\times N_G$, and $N_H\times N_H$, respectively. Matrix I_ξ is of dimension $N_F\times N_W$. I_η has dimension $N_G\times N_W$. Finally, I_θ is of dimension $N_H\times N_W$.

The systems of equations (3.2.32), (3.2.37), (3.2.39) - (3.2.41) are combined into an overall matrix equation, resulting in a reduced-order model describing the evolution of the temporal coefficients in the POD expansions (3.2.21) - (3.2.25). The reduced order model is of the form

$$\begin{bmatrix}\dot{\alpha}\\ \beta\\ \xi\\ \eta\\ \theta\end{bmatrix}=\begin{bmatrix}A_\alpha & 0 & 0 & 0 & 0\\ I_\beta & A_\beta & 0 & 0 & 0\\ 0 & I_\xi & A_\xi & 0 & 0\\ 0 & I_\eta & 0 & A_\eta & 0\\ 0 & I_\theta & 0 & 0 & A_\theta\end{bmatrix}\begin{bmatrix}\alpha\\ \beta\\ \xi\\ \eta\\ \theta\end{bmatrix}+\begin{bmatrix}B_\alpha\\ 0\\ 0\\ 0\\ 0\end{bmatrix}u(t)+\begin{bmatrix}0\\ F_\beta\\ 0\\ 0\\ 0\end{bmatrix}f(t). \tag{3.2.42}$$

The reduced model is completed with an initial condition $[\alpha(0)\ \ \beta(0)\ \ \xi(0)\ \ \eta(0)\ \ \theta(0)]^T$.

3.2.6 Reduced Model Results

Utilizing the reduced-order model in (3.2.42) requires the construction of a split-POD basis. The high-dimensional discretized supply chain model given by (3.2.12) is used to generate instantaneous snapshots for the system with and without boundary actuation. To generate a baseline POD basis capable of spanning dynamics resulting from a variety of initial conditions, baseline data is generated by prescribing several nonzero initial profiles for concentration $C_W(t,x)$. Profiles specified are of the form

$$\begin{aligned} &C_W(0,x) \equiv 3, && C_W(0,x) = 3\frac{x}{L}, \\ &C_W(0,x) = -3\frac{x}{L} + 3, && C_W(0,x) = 3sin\left(\frac{\pi x}{L}\right), \\ &C_W(0,x) = \frac{1}{2}\left[cos\left(\frac{2\pi x}{L}\right) + 1\right]. \end{aligned} \tag{3.2.43}$$

For each case specified in (3.2.43), the concentration of species V is initially held at zero. In addition, the concentrations of the three daughter species F, G, and H are initially held at their steady-state profiles that result from the nominal supply chain configuration. Simulated data is generated for each initial configuration from $t = 0.2$ to $t = 75$ in increments of $\Delta t = 0.2$. Snapshots generated for all five species concentrations are collected into a single snapshot ensemble. A baseline POD basis consisting of four modes captures 99.9 percent of the baseline data variability. The baseline POD basis is shown in Figure 3.15(a).

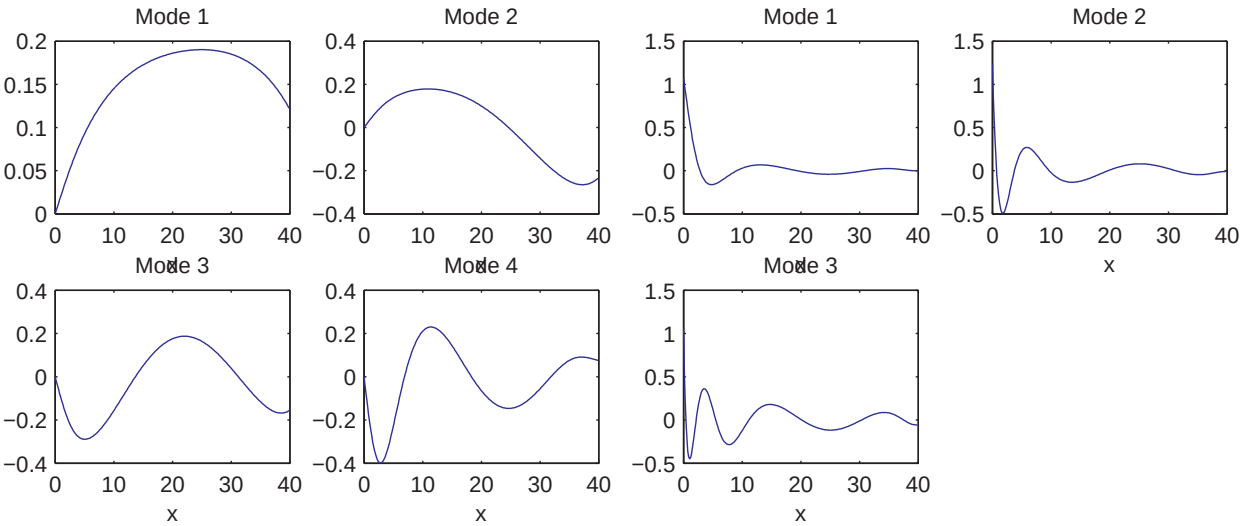

(a) Baseline POD Basis

(b) Actuator POD Basis

Figure 3.15. The Baseline and Actuator POD Bases

With the baseline basis in hand, data is generated for the solution with nonzero boundary

actuation. Each species is held at its nominal concentration profile initially. To generate a rich actuated ensemble over a range of input frequency, chirp inputs of the form

$$u(t) = 10\left|sin\left(\frac{t^2}{10}\right)\right|, \qquad u(t) = 0, \qquad u(t) = 10\left|sin\left(\frac{t^2}{10}\right)\right|, \tag{3.2.44}$$
$$f(t) = 0 \qquad f(t) = 10\left|sin\left(\frac{t^2}{10}\right)\right| \qquad f(t) = 10\left|sin\left(\frac{t^2}{10}\right)\right|$$

are specified for boundary conditions (3.2.6)-(3.2.7). Data for each of the three actuated cases are generated from $t = 0.2$ to $t = 75$ in increments of $\Delta t = 0.2$. The three sets of actuated data are then combined to yield an overall actuated snapshot ensemble. Split-POD is performed on this ensemble of actuated data. An actuator basis consisting of 3 modes captures 99.9 percent of new variability induced by boundary actuation. The basis of actuator modes is shown in Figure 3.15(b).

The baseline and actuated bases are combined into an overall basis as in (2.3.9). The combined basis consists of 7 modes - 4 baseline modes and 3 actuator modes. As the daughter concentrations $C_F(t,x)$, $C_G(t,x)$, and $C_H(t,x)$ are specified to have homogeneous boundary conditions in the distributed parameter system, only the baseline modes are used in the expansions for these concentrations. As a result, $N_F = N_G = N_H = 4$ in (3.2.23) -

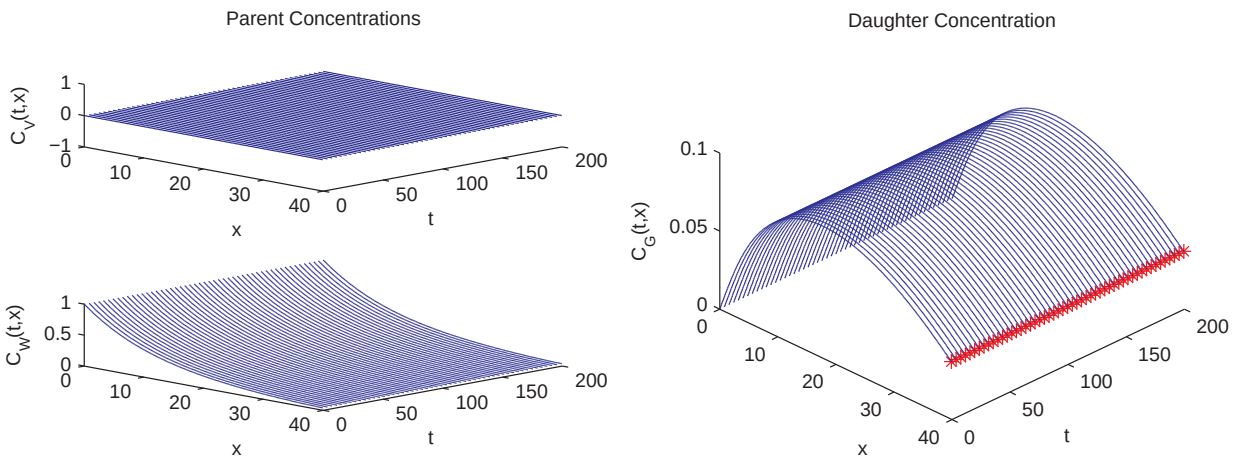

(a) Reduced-Order Nominal Dynamics for Species V (b) Reduced-Order Nominal Dynamics for Species G and W

Figure 3.16. Reduced-Order Nominal Supply Chain Dynamics

(3.2.25). Parent concentrations $C_V(t,x)$ and $C_W(t,x)$ have time-varying boundary conditions at $x = 0$. Thus, the full combination of baseline and actuated bases is used in their mode expansions. This results in $N_V = N_W = 7$ in (3.2.21) - (3.2.22). With the spatial resolution used in the simulations, the full-dimensional discretized system in (3.2.12) describes 1,330

state variables. With the split-POD basis shown in Figure 3.15, the reduced-order model in (3.2.42) describes only 26 state variables, resulting in significant reduction in the dimension of the state-space representation.

The ability of the reduced-order model to reproduce the nominal chemical profile configuration in seen in Figure 3.16. As was the case for the highly discretized supply chain model, a nominal value of $f(t) = 1$ results in the target value of $C_G(t, 40) = 0.0372$. As was done before, the desired concentration of species G is denoted by asterisks at $x = 40$ in the plot of $C_G(t, x)$. By comparing the results of Figure 3.16 to the full-order nominal results shown in Figure 3.9, it is seen that there is virtually no difference between the reduced and full-order solutions for the nominal configuration.

The behavior of the disrupted reduced-order model with no control is shown in Figure 3.17. As was seen before, the severe disruption in the supply of species W causes the

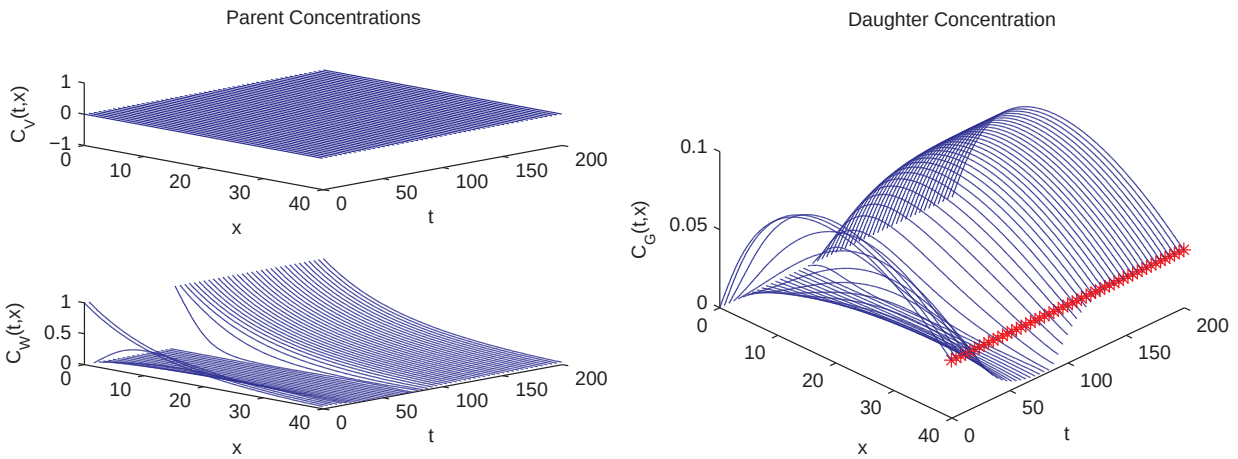

(a) Reduced-Order Disturbed Dynamics for Species V and W

(b) Reduced-Order Disturbed Dynamics for Species G

Figure 3.17. Reduced-Order Disturbed Supply Chain Dynamics

concentration of species G to depart significantly from its target value at $x = 40$. By comparing the disturbance results of Figure 3.17 to the full-order disturbance results shown in Figure 3.10, it is apparent that there is very good agreement between the reduced and full-order models for the disturbed case. The impact of the disruption on the reduced-order model is more clearly seen in Figure 3.18. As before, the dashed curve denotes the desired value of $C_G(t, 40)$. The solid curve denotes the value attained for $C_G(t, 40)$ in the disrupted supply chain. In the reduced model, the disruption causes $C_G(t, 40)$ to depart significantly from its target value. As is evident by comparing Figure 3.18 and Figure 3.11, the departure predicted by the reduced-order chemical supply chain model is similar to that obtained by the full-order system.

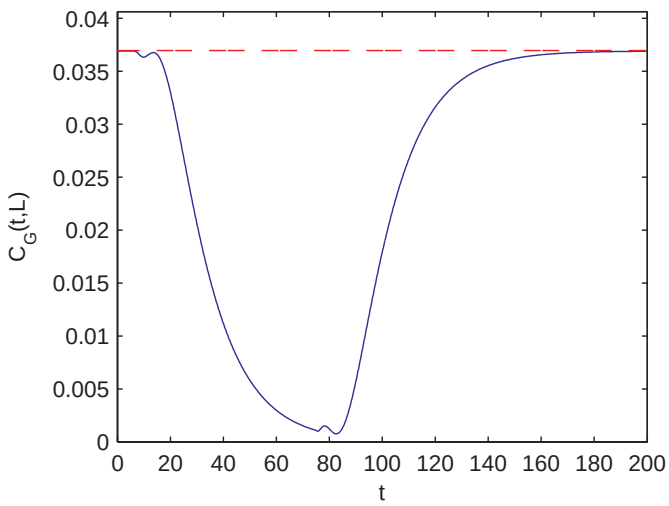

Figure 3.18. Departure of Species G from the Target Value After Disruption for the Reduced Model

3.2.7 Controlled Reduced Model

The tracking LQR formulation in (2.2.7) is now used to develop a feedback controller for the reduced-order supply chain model. As the reduced-order model describes the evolution of the POD temporal coefficients in basis expansions (3.2.21) - (3.2.25), the reduced-order feedback controller must act on these coefficients. In the full-dimensional control problem, large state-weights could be placed on states over specific locations in the interval $[0, L]$ to emphasize the control of these states in the control problem. This is not the case for the reduced model. POD modes are defined over the entire interval $[0, L]$. As a result, controlling a particular POD temporal coefficient potentially has an impact over the entire interval. In order to formulate the reduced-order control problem so that the concentration of species G at $x = 40$ maintains its target value during a disruption, a reference steady-state profile is generated for $C_G(t, x)$. To ensure that this concentration profile provides an attainable control objective, it is obtained after specifying a zonzero constant value for $C_V(t, 0)$ with $C_W(t, 0)$ fixed at zero. The subsequent steady-state profile for $C_G(t, x)$ is calculated and scaled so that it satisfies the target value at $x = 40$. The scaled steady-state profile is used as the reference condition in the reduced-order control problem. The particular reference profile used in the results that follow is shown in Figure 3.19. This profile is projected onto the POD basis for concentration $C_G(t, x)$, resulting in reference temporal coefficients in the tracking LQR cost function (2.2.7). As discussed previously, only the four baseline POD modes are used in the basis expansion of $C_G(t, x)$ given by (3.2.24). The weights prescribed on the temporal coefficients for these modes in the control problem are 15,000, 1,000, 100, and 100 for $\eta_1(t)$, $\eta_2(t)$, $\eta_3(t)$, and $\eta_4(t)$, respectively. All other temporal coefficients in the reduced model are prescribed weights of zero. Unit weight is specified for the control input. The dynamics of the controlled reduced-order model are shown in Figure 3.20.

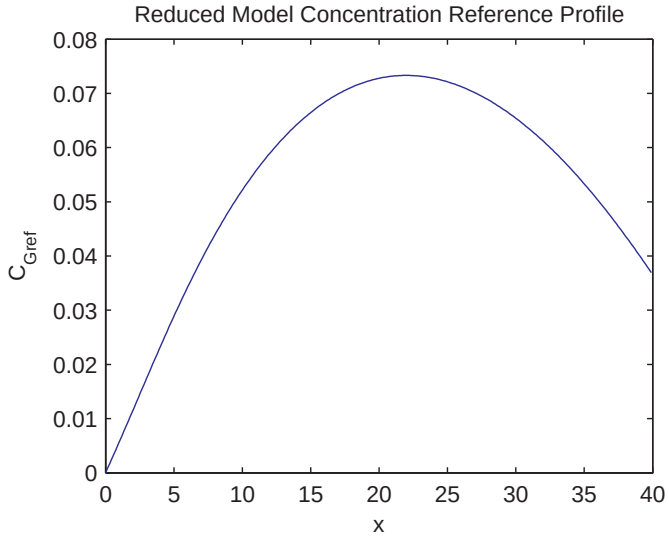

Figure 3.19. Concentration Reference Profile for the Reduced-Order Control Problem

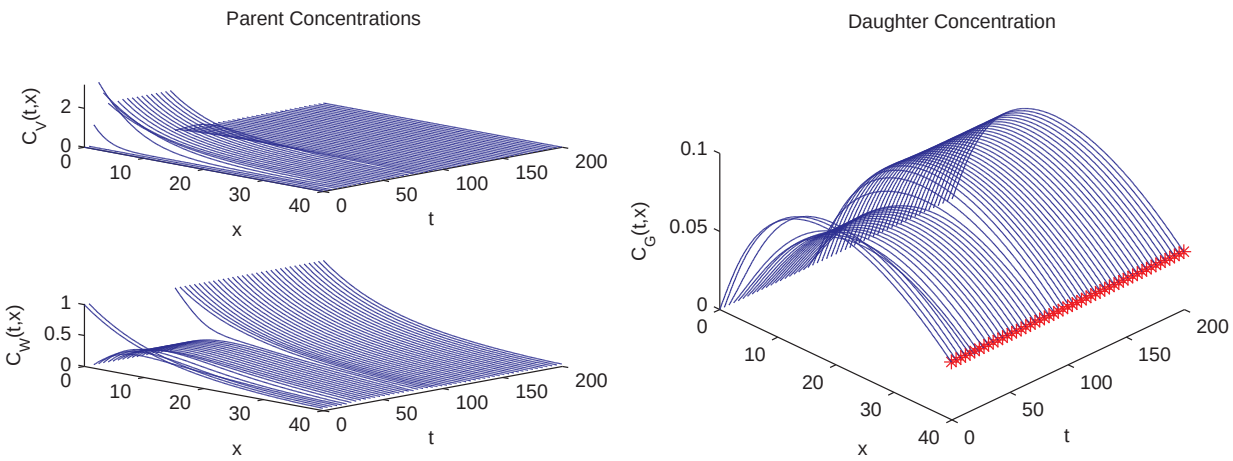

(a) Reduced-Order Controlled Dynamics for Species V and W

(b) Reduced-Order Controlled Dynamics for Species G

Figure 3.20. Reduced-Order Disturbed Supply Chain Dynamics with Control

As seen in Figure 3.20(a), the feedback controller automatically compensates for the disruption in the availability of species W. This allows $C_G(t, 40)$ to remain near its target value until the supply of species W is gradually brought back online. Once $C_W(t, 0)$ returns to its nominal value, the control input becomes zero, allowing species V to gradually dissipate

from the system. The controlled results obtained for the reduced-order model are quite similar to those obtained for the full-order system, as is evident by comparing Figure 3.20 to Figure 3.13. The ability of the controller to effectively maintain the target condition in the reduced-order model is more clearly seen in Figure 3.21. As seen in that figure, the target

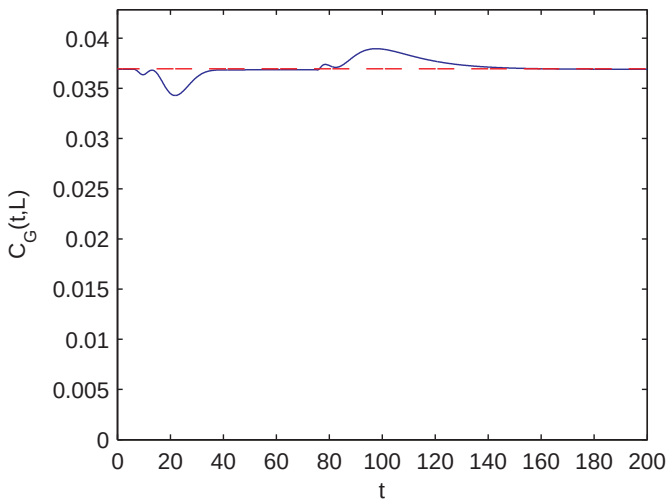

Figure 3.21. Departure of Species G from the Target Value After Disruption for the Reduced Model with Control

value is maintained fairly well. There are slight deviations from the target value near the start and end of the disruption. These deviations are due to the controller being unable to assume negative values. Near the beginning and end of the disruption, negative values for $C_V(t, 0)$ resulting from optimal control law (2.2.8) are overwritten with a value of zero as negative concentration values do not make physical sense. This leads to deviations when the boundary input can not assume it optimal value determined from the feedback control law. A control formulation able to provide a strictly non-negative optimal feedback controller would likely reduce or eliminate the deviation from the target state.

3.2.8 High-Dimensional Tracking

To validate the utility of the feedback controller developed from the reduced-order model, it must be incorporated and tested in the full-order system. This requires that it be implemented in the full-order dynamical system (2.2.2)-(3.2.14). One can not directly incorporate the reduced-order controller in the full-order system model, however. Controllers obtained via the reduced-order model act on POD temporal coefficients. As a result, one must project the full-order solution at each time step onto the POD basis to obtain temporal coefficients on which the reduced-order control can act. As the control input enters the system by way of a time-varying boundary condition, a technicality must be resolved. The POD basis modes used to construct the reduced-order model cover the entire spatial domain, including the

boundary. To project the full-order solution onto the POD basis, all boundary conditions must be specified for the full solution prior to the projection. As a result, the projection of the full-order solution with boundary data onto the POD modes requires that the boundary control in the full-order solution be specified beforehand. In effect, the boundary input due to the controller needs to be specified before it has been calculated, a seeming impossibility. We overcome this difficulty by utilizing a fixed-point subiteration [30] to project the full-order solution onto the POD basis at each time step. With the temporal coefficients obtained via this subiteration in hand, the reduced-order control is implemented in the full-order system. The dynamics of the full-order system driven by the reduced-order feedback controller found previously are shown in Figure 3.22. By comparing the closed-loop dynamics of Figure 3.22

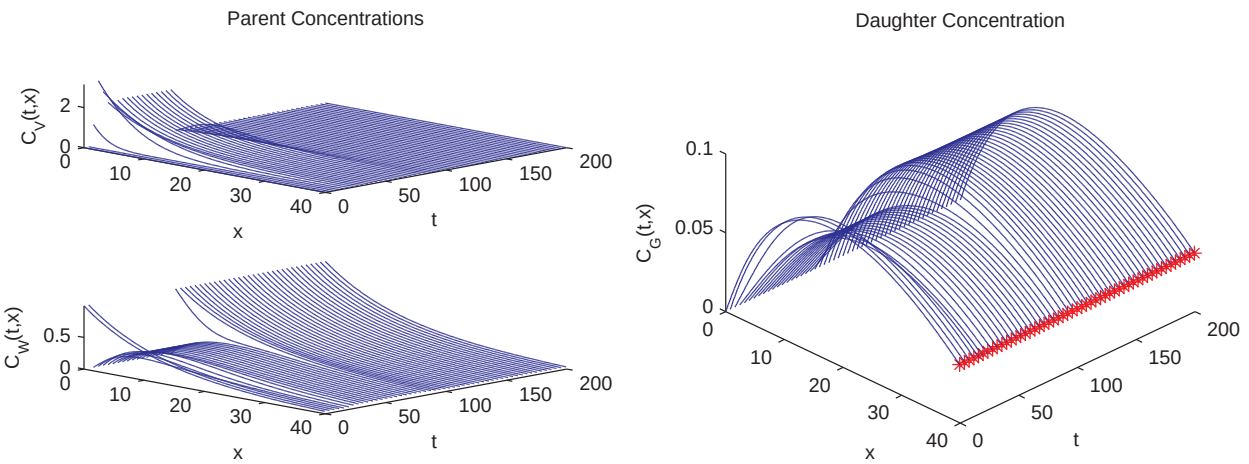

(a) Full-Order Controlled Dynamics for Species V and W with Reduced-Order Control Implementation

(b) Full-Order Controlled Dynamics for Species G with Reduced-Order Control Implementation

Figure 3.22. Controlled Full-Order Supply Chain Dynamics with Reduced-Order Control Implementation

to the reduced-order results of Figure 3.20, it is evident that there is very good agreement between the reduced and full-order models under feedback. The reduced and full-order results are virtually identical. The reduced-order controller is able to control the full-order system quite nicely, and the dynamics of the full-order system under feedback are predicted well by the closed-loop reduced model.

The good agreement between the full and reduced-order models under feedback is also apparent in the results of Figure 3.23. When implemented in the full-order system, the reduced-order controller maintains the target condition as predicted by the closed-loop reduced-order model. The results of Figure 3.23 and Figure 3.21 are almost identical. In both cases, the deviation from the target near the beginning and end of the disruption is due to the inability of the controller to assume negative values. The feedback controller designed from a reduced-order model with 26 unknowns is able to effectively control the full-order discretized system describing 1,330 state variables. The relevance to multi-dimensional or very large chemical

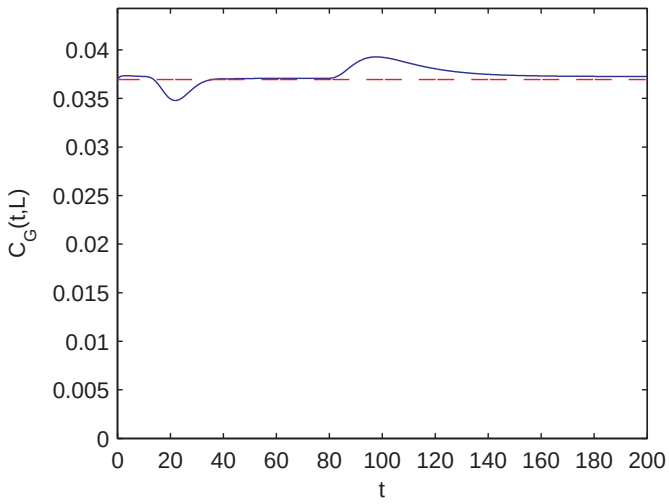

Figure 3.23. Departure of Species G from the Target Value After Disruption for the Full-Order Model with Reduced-Order Control

supply chains is obvious. Using control design techniques to perform resilience analysis on very large systems requires a reduction of the system order. The reduced model can then be used to develop suitable controllers for the full-order system.

These results illustrate the advantages of reduced-order modeling when applied to systems that yield exceedingly large discretized models. If done carefully, system dimension can be reduced by several orders of magnitude with very little loss in accuracy. The significant reduction of system order greatly reduces the computational burden associated with simulating these systems. Moreover, order reduction enables investigations of system stability and optimal feedback control design for configurations in which these pursuits are computationally intractable when attempted on the full-order system. This enables resilience analysis using control design methods for configurations in which these pursuits would be computationally intractable when attempted on the full-dimensional system.

Chapter 4

Summary and Future Work

Critical infrastructure resilience has become a national priority for the U. S. Department of Homeland Security. For this project we investigated the development of quantitative resilience analysis methods through control design. Specifically, we developed a decision process that resilience analysts can use to identify a suitable control method when performing quantitative resilience analysis. The selection of a control method is dependent upon the characteristics of the model used to represent the infrastructure system. Additionally, we applied control methods to two sets of representative infrastructure systems to demonstrate how control methods can be utilized to perform resilience analysis.

The development of quantitative resilience methods still requires much work. Some of the technical work to be done includes:

- **Apply control methods, similar to those demonstrated in Chapter 3, to more detailed, complex infrastructure system models**: The models used in this project were representative of generic infrastructure systems. Demonstrating that control methods can be applied to an actual national infrastructure system, e.g., the national petrochemical supply chain, could be useful in further vetting how control methods can be used for CIR analysis.

- **Leverage infrastructure expertise to develop customized control methods for nonlinear systems**: Control of highly nonlinear systems cannot be approximated well through linearization. For these types of systems, it may be necessary to develop customized control methods.

- **Investigate the use of optimization methods to use for resilience analysis**: Any optimal control problem can be posed as a more general optimization problem. The use of optimal feedback control algorithms can make solution of these problems more efficient, but the application of these methods requires linearity of the system. When it is not possible or preferable to apply or develop a nonlinear control method, nonlinear optimization methods can be utilized. It would be worthwhile to investigate the use of nonlinear optimization techniques for resilience analysis methods.

References

[1] Reagan, R., *Executive Order 13282, National Security Telecommunications Advisory Committee*, Washington, D.C., 1982.

[2] Clinton, W., *Presidential Decision Directive PDD-63, Protecting America's Critical Infrastructures*, Washington, D.C., 1998.

[3] Bush, G. W., *Homeland Security Presidential Directive-3 (HSPD-3)*, Washington, D.C., 2002.

[4] Bush, G. W., *Homeland Security Presidential Directive-7 (HSPD-7)*, Washington, D.C., 2003.

[5] Vugrin, E. D., Warren, D. E, Ehlen, M. A., and Camphouse, R. C., "A Framework for Assessing the Resilience of Infrastructures and Economic Systems," to appear in *Sustainable Infrastructure Systems: Simulations, Imaging, and Intelligent Engineering*, Springer-Verlag, New York, 2010.

[6] Vugrin, E. D., Camphouse, R. C., Downes, P. S., Ehlen, M. A., and Warren, D. E, "Measurement of System Resilience: Application to Chemical Supply Chains," extended abstract for *Proceedings of SIAM Conference on Mathematics for Industry: Challenges and Frontiers*, San Francisco, October 9-10, 2009.

[7] Astrom, K., and Hagglund, T., *Advanced PID Control*, Instrumentation, Systems, and Automation Society, Research Triangle Park, NC, 2006.

[8] Kirk, D., *Optimal Control Theory*, Dover Publications, New York, 2004.

[9] Haddad, W. M., and Chellaboina, V., *Nonlinear Dynamical Systems and Control*, Princeton University Press, 2008.

[10] Ljung, L., "Perspectives on System Identification", *Proceedings of 2008 International Federation of Automatic Control*, Seoul, 2008.

[11] Zhou, K. and Doyle, J. C., *Robust and Optimal Control*, Prentice Hall, New Jersey, 1996.

[12] Djouadi, S.M., Camphouse, R.C., and Myatt, J.M., "Empirical Reduced-Order Modeling for Boundary Feedback Flow Control," *Journal of Control Science and Engineering*, Volume 2008, Article ID 154956.

[13] Khalil, H.K., *Nonlinear Systems*, Prentice Hall, Inc., New Jersey, 2002.

[14] Sandell, N., Jr., Varaiya, P., Athans, M., and Safanow, M. G., "A Survey of Decentralized Control Methods for Large Systems," *IEEE Transactions on Automatic Control*, Vol. 23, No. 2, April 1978.

[15] Ye, H., Michel, A. N., and Hou, L., "Stability Theory for Hybrid Dynamical Systems," *IEEE Transactions on Automatic Control*, 43(4), 1998.

[16] Zhang, J., Johansson, K. H. , Lygeros, J., and Sastry, S., *Dynamical Systems Revisited: Hybrid Systems with Zeno Executions*, volume 1790, pages 451–464. Springer-Verlag, Berlin Heidelberg, 2000.

[17] Lafferriere, G., Pappas, G. J. and Sastry, S. " O-Minimal Hybrid Systems," *Math. Control Signals Systems*, Vol. 13, 2000, pp 1-21.

[18] Ramadge, P. J. G. , and Wonham W. M., "The Control of Discrete Event Systems," *Proceedings of the IEEE*, 77(1), January 1989.

[19] Antoulas, A., *Approximation of Large-Scale Dynamical Systems*, Society for Industrial and Applied Mathematics, Philadelphia, 2005, pp. 2-24.

[20] Holmes, P., Lumley, J., and Berkooz, G., *Turbulence, Coherent Structures, Dynamical Systems and Symmetry*, Cambridge University Press, New York, 1996, pp. 86-127.

[21] Sirovich, L., "Turbulence and the Dynamics of Coherent Structures, Parts I-III," *Quarterly of Applied Mathematics*, Volume 45, Brown University, Rhode Island, 1987, pp. 561-590.

[22] Camphouse, R. C. et al, "A Snapshot Decomposition Method for Reduced Order Modeling and Boundary Feedback Control," AIAA Paper 2008-4195, June 2008.

[23] Debnath, L. and Mikusiński, P., *Introduction to Hilbert Spaces with Applications*, Academic Press, California, 1999, pp. 87-130.

[24] Wallace, R. D., Andino, M. Y., Glauser, M. N., Schmit, R. F., Camphouse, R. C., and Myatt, J. H., "Flow and Aero-Optics Around a Turret Part 2: Surface Pressure Based Proportional Closed-Loop Flow Control," AIAA Paper 2008-4217, June 2008.

[25] Sterman, J. D., *Business Dynamics: Systems Thinking and Modeling for a Complex World*, Irwin McGraw-Hill, Boston, 2000.

[26] Banks, H. T. and Burns, J. A., "Hereditary Control Problems: Numerical Methods Based on Averaging Approximations," *SIAM J. Control and Optimization*, Vol. 16, 1978, pp 169-208.

[27] Gibson, J. S., "Linear-Quadratic Optimal Control of Hereditary Differential Systems: Infinite Dimensional Riccati Equations and Numerical Approximations," *SIAM J. Control and Optimization*, Vol. 21, 1983, pp 95-139.

[28] Kappel, F., " Approximation of LQR-Problems for Delay Systems: A Survey," in *Computation and Control II*, K. Bowers and J. Lund, eds., Birkhauser, Cambridge, 1991, pp 187-224.

[29] Rosen, I. G., " Convergence of Galerkin Approximations for Operator Riccati Equations-A Nonlinear Evolution Equation Approach," *J. Math. Anal. Appl.*, Vol. 155, 1991, pp 226-248.

[30] Camphouse, R.C., "Boundary Feedback Control Using Proper Orthogonal Decomposition Models," *Journal of Guidance, Control, and Dynamics*, Vol. 28, No. 5, September-October 2005, pp 931-938.

[31] Camphouse, R. C. and Myatt, J. H., "Reduced Order Modeling and Boundary Feedback Control of Nonlinear Convection," AIAA Paper 2005-5844, August 2005.

[32] Camphouse, R. C., Djouadi, S.M., and Myatt, J. H., "Feedback Control for Aerodynamics," 2006 Conference on Decision and Control.

[33] Carlson, H., Glauser, M., and Roveda, R., "Models for Controlling Airfoil Lift and Drag," AIAA Paper 2004-0579, January 2004.

[34] Kasnakoğlu, C., Serrani, A., and Efe, M., "Control Input Separation by Actuation Mode Expansion for Flow Control Problems," *International Journal of Control*, 81 (9):1475-1492, 2008.

[35] Kasnakoğlu, C., Camphouse, R.C., and Serrani, A., "Reduced-order Model-based Feedback Control of Flow over an Obstacle Using Center Manifold Methods," *Journal of Dynamic Systems, Measurement and Control*, Volume 131, Issue 1, January 2009.

DISTRIBUTION:

1	MS 1318	Bart van Bloemen Waanders, 01414 (electronic)
1	MS 1138	Pablo Garcia, 06320 (electronic)
1	MS 1138	Lillian Snyder, 06321 (electronic)
1	MS 1138	Eric Vugrin, 06321 (electronic)
1	MS 1138	Mark Ehlen, 06321 (electronic)
1	MS 1138	Drake Warren, 06321 (electronic)
1	MS 1138	Sue Downes, 06321 (electronic)
1	MS 1138	Munaf Aamir, 06321 (electronic)
1	MS 1138	Nancy Brodsky, 06321 (electronic)
1	MS 1138	Theresa Brown, 06321 (electronic)
1	MS 1138	Verne Loose, 06321 (electronic)
1	MS 1138	Vanessa Vargas, 06321 (electronic)
1	MS 1138	Dan Pless, 06321 (electronic)
1	MS 1138	Dan Horschel, 06322 (electronic)
1	MS 1138	Arlo Ames, 06322 (electronic)
1	MS 1138	Ray Trechter, 06323 (electronic)
1	MS 1138	Keith Bauer, 06324 (electronic)
1	MS 1138	Ellen Lemen, 06325 (electronic)
1	MS 1138	Steve Kleban, 06326 (electronic)
1	MS 1138	Daniel Sunderland, 06326 (electronic)
1	MS 0734	Bruce Kelly, 06327 (electronic)
1	MS 1188	Kay Vugrin, 06342 (electronic)
1	MS 1395	David Kessel, 06710 (electronic)
1	MS 1395	Moo Lee, 06711 (electronic)
1	MS 1395	Chris Camphouse, 06711 (electronic)
1	MS 0484	Russ Skocypec, 08004 (electronic)
1	MS 9151	Howard Hirano, 08960 (electronic)
1	MS 9159	Heidi Ammerlahn, 08962 (electronic)
1	MS 9159	Lynn Yang, 08962 (electronic)
1	MS 9159	David Franco, 08962 (electronic)
1	MS 0899	Technical Library, 9536 (electronic)
1	MS 0123	D. Chavez, LDRD Office, 1011

Sandia National Laboratories